

---

# A Textbook Remedy for Domain Shifts: Knowledge Priors for Medical Image Analysis

---

Anonymous Author(s)

Affiliation

Address

email

## Abstract

1 While deep networks have achieved broad success in analyzing natural images,  
2 when applied to medical scans, they often fail in unexcepted situations. We  
3 investigate this challenge and focus on model sensitivity to domain shifts, such as  
4 data sampled from different hospitals or data confounded by demographic variables  
5 such as sex, race, etc, in the context of chest X-rays and skin lesion images.  
6 A key finding we show empirically is that existing visual backbones lack an  
7 appropriate prior from the architecture for reliable generalization in these settings.  
8 Taking inspiration from medical training, we propose giving deep networks a prior  
9 grounded in explicit medical knowledge communicated in natural language. To this  
10 end, we introduce **Knowledge-enhanced Bottlenecks (KnoBo)**, a class of concept  
11 bottleneck models that incorporates knowledge priors that constrain it to reason  
12 with clinically relevant factors found in medical textbooks or PubMed. KnoBo uses  
13 retrieval-augmented language models to design an appropriate concept space paired  
14 with an automatic training procedure for recognizing the concept. We evaluate  
15 different resources of knowledge and recognition architectures on a broad range  
16 of domain shifts across 20 datasets. In our comprehensive evaluation with two  
17 imaging modalities, KnoBo outperforms fine-tuned models on confounded datasets  
18 by 32.4 % on average. Finally, evaluations reveal that PubMed is a promising  
19 resource for making medical models less sensitive to domain shift, outperforming  
20 other resources on both diversity of information and final prediction performance.

## 21 1 Introduction

22 Robustness to domain shifts is a key property for models operating on medical images because  
23 transfer scenarios arise widely. Deep networks have achieved broad success in analyzing natural  
24 images (everyday human contexts), but when applied to medical scans, they often substantially  
25 degrade under distribution shift [86, 15]. Medical datasets are small, and unidentified confounds in  
26 them combined with model misspecification can dramatically degrade performance [46, 21, 24]. Such  
27 failure erodes confidence as models do not learn the right information from training data, hampering  
28 adoption by medical professionals. We study such problems by investigating the performance of  
29 systems in the presence of confounded data and address a main shortcoming we discover.

30 Model sensitivity to domain shift can be measured by introducing synthetic confounds into data  
31 and evaluating on samples where the confound misleads the model. For example, in Figure 1, we  
32 introduce confounded datasets for chest X-ray and skin lesion images where, during training, positive  
33 data is sampled from one group and negative from another. This association is reversed at testing  
34 time, creating an adversarial out-of-distribution (OOD) evaluation. In 5 such constructed confounds  
35 per modality, covering scenarios of race, sex, age, scan position, and hospital, we find models unable  
36 to generalize well, dropping over 63% on average over an in-distribution (ID) evaluation.

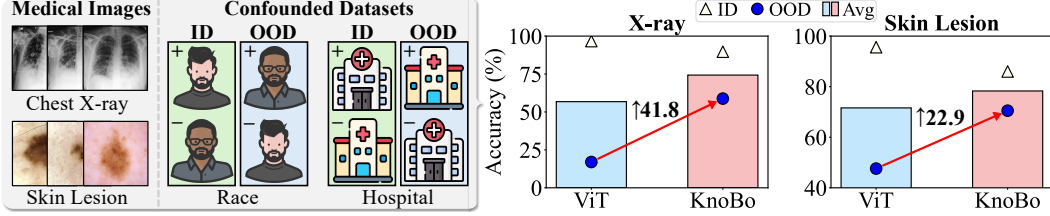


Figure 1: In-domain (ID), out-of-domain (OOD), and average of ID and OOD (Avg) performance on confounded medical image datasets. Our interpretable **Knowledge-enhanced Bottlenecks (KnoBo)** are more robust to domain shifts (e.g., race, hospital, etc) than fine-tuned vision transformers [17].

Priors are an important signal allowing models to adopt appropriate hypotheses in low or misleading data regimes. We hypothesize that existing visual backbones lack an appropriate prior for robust generalization in medicine. Like previous work identifying that vision backbones have a deep image prior even when entirely untrained [72, 78], we compare the quality of image representations produced by untrained networks on natural versus medical images. Given the output from a frozen untrained visual backbone, we train a linear classifier for predicting a diversity of labels (see Figure 2). Across architecture, these untrained models are higher quality featurizers of natural images than directly using pixels as features. In contrast, **across multiple medical modalities, the deep image prior in current major visual backbones is no more effective than using pixels (and often worse).**

To address the lack of an effective deep image prior for medical images, we propose using an inherently interpretable model design. We draw inspiration from medical education, where students first learn from textbooks and later in a more practical setting during the residency with an attending doctor. Our models mimic this pattern: first, documents are used to identify important knowledge, and then they learn by example from data. We employ concept bottleneck models (CBMs) [41] and enrich them with information derived from resources broadly accessible to medical students. CBMs are a class of inherently interpretable models that factor model decisions into human-readable concepts that are combined linearly. Our methods build on recent approaches for language model (LM) guided bottleneck construction where LMs are prompted for discriminative attributes [90].

We introduce **Knowledge-enhanced Bottlenecks (KnoBo)** to incorporate knowledge priors that encourage reasoning with factors found in medical documents. KnoBo extends CBMs to medical imaging and employs retrieval-augmented generation into concept design. For example, we extract concepts from medical textbooks as natural language questions like *Is there ground-glass opacity?* to help the model classify whether an X-ray is positive for a respiratory infection. As illustrated in Figure 3, KnoBo factors learning into three parts: (1) an interpretable bottleneck predictor, (2) a prior over the structure of the bottleneck, and (3) a prior over predictor parameters. This factorization allows us to guide the model with a prior rooted in medical documents. The approach relies on an iterative retrieval process where an LM summarizes documents to propose concepts, forming our medical image prior (Sec 4.2). Given the concepts, a pretraining corpus of reports and images is used to construct a classifier for a concept (Sec 4.3). Finally, a CBM is learned using predictions from classifiers on data while regularized by a prior formed from LM generations. (Sec 4.4).

We evaluate KnoBo on our benchmark of confounded tasks. Averaged over confounds, KnoBo increases OOD performance by 41.8% and 22.9% on X-ray and skin lesion datasets, respectively. KnoBo’s success in OOD performance comes at little sacrifice in ID settings, providing a better model overall when averaging the two data settings. We also explore 5 different sources of knowledge and reveal that PubMed outperforms other resources in terms of both diversity of information and final prediction performance. Overall, our work demonstrates that a key missing ingredient for robustness to distribution shift in medical imaging models is a prior rooted in knowledge.

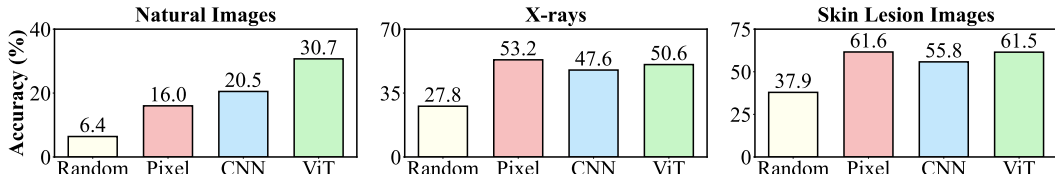


Figure 2: Classification performance on natural and medical images through linear probing using features extracted from untrained and frozen models versus pixels features (See Sec 3 for details).

## 74 2 Related Work

75 The rapid advancement in medical foundation models offers the opportunity to develop healthcare  
 76 AI [55, 49]. However, their lack of transparency presents risks in real-world applications [5].  
 77 **Interpretability** is crucial for using models in high-stakes domains [30, 79, 87]. Previous work  
 78 has primarily focused on post-hoc interpretability [76, 95, 29, 75], which may not provide faithful  
 79 explanations [69]. As an alternative, inherently interpretable methods produce explanations that  
 80 align with the model’s reasoning processes [8, 3]. In this work, we build upon **Concept Bottleneck**  
 81 **Models** (CBMs) [41], which predict by linearly combining human-designed concepts. Recent work  
 82 [91, 60, 90] scales the applications of CBMs by aligning concepts and images with CLIP [64]  
 83 and prompting language models to generate concept bottlenecks automatically. In our work, we  
 84 treat CBMs as the architecture to incorporate knowledge priors for mitigating medical domain shift  
 85 problems. Our bottlenecks, built from the medical corpus, are attributable and more trustworthy.

86 **Domain Generalization and Robustness** are critical in medical domains where the distribution  
 87 of imaging protocols, devices, and patient populations can significantly vary [25]. A line of work  
 88 studies various domain-shift problems [42, 2], proposing algorithms to learn invariant representations  
 89 [57, 22, 80, 63] and employing domain/group information for reweighting [71, 93, 44, 96]. However,  
 90 many studies show those methods do not improve over standard Empirical Risk Minimization (ERM)  
 91 [67, 26, 33, 27]. Fine-tuning the last layer [68, 40] or selectively fine-tuning a few layers [47] is  
 92 sufficient for robustness against spurious correlations in those datasets. We address domain shifts in  
 93 medical imaging from a novel perspective by employing interpretable models to integrate knowledge  
 94 priors. Our approach encourages models to adhere to diagnostic rules similar to those doctors use  
 95 rather than relying on spurious correlations. Concurrent work shows bottleneck models can perform  
 96 well on out-of-domain X-ray data but severely reduced in-domain performance as a consequence [89].  
 97 In contrast, we demonstrate a significantly better compromise between OOD and ID performance,  
 98 using a broader set of modalities and constructing our bottlenecks from medical documents.

99 **Knowledge Rich Multimodal Reasoning.** Knowledge plays an important role in clinical diagnosis  
 100 [6]. Some multimodal tasks [82, 53, 74] require models to use explicit outside knowledge to make  
 101 correct predictions. Previous methods [52, 50, 31] retrieve documents for each example from the  
 102 external knowledge base as context for models to generate the answer. Our work focuses on leveraging  
 103 knowledge in medical image classification. **Retrieval-Augmented Generation** [48, 23] has been  
 104 shown to be beneficial for knowledge-intensive tasks [38], including biomedicine [20, 84]. The  
 105 retrieved medical documents are either used as context during inference [88] or data for pretraining  
 106 [94]. In contrast, we treat documents as background knowledge for large language models to build  
 107 concept bottlenecks. Instead of retrieving documents for every input, we build a global knowledge  
 108 prior from a medical document corpus, which is shared across all examples.

## 109 3 Deep Image Priors for Medical Images

110 This section revisits the concept of deep image priors [72, 78], i.e., some data-agnostic assumptions  
 111 from model structure, in the context of image classification across various domains. By comparing  
 112 linear probing using features extracted by untrained deep networks against pixel-based features, we  
 113 observe that existing vision backbones lack suitable priors for medical domains. This observation  
 114 motivates our knowledge-enhanced bottlenecks (Sec 4) to integrate more robust priors into models.

115 **Setup.** Consider a dataset of image-label pairs,  $\mathcal{D} = \{(I, y)\}$ , where  $I$  is an image and  $y \in \mathcal{Y}$   
 116 denotes the label from one of  $N$  classes. The model learns to predict  $P(y|I, \theta)$ , where  $\theta$  is the model  
 117 parameters. We employ a frozen, untrained vision backbone  $\mathcal{V}$  to extract features from  $I$ , producing a  
 118 feature vector  $\mathbf{x} = \mathcal{V}(I)$ , where  $\mathbf{x} \in \mathbb{R}^d$ . A linear mapping function  $f_\theta : \mathbb{R}^d \rightarrow \mathcal{Y}$  is then trained to  
 119 classify these features into label spaces. In this case, the model parameters  $\theta$  will inherit the implicit  
 120 architectural priors of  $\mathcal{V}$ . As a baseline, we extract a subset of  $d$  pixels directly from the image as  
 121 the feature without any model-based priors, represented as  $\mathbf{x}_p \in \mathbb{R}^d$ . We compare the classification  
 122 performance using  $\mathbf{x}$  versus  $\mathbf{x}_p$  to probe the efficacy of the vision backbone’s priors.

123 **Experiments.** We evaluate two state-of-the-art vision backbones, ViT-L/14 [17] and ConvNext-L  
 124 [51], on three categories of images: natural photos (e.g., ImageNet [70]), X-rays (e.g., NIH-CXR  
 125 [83]), and skin lesion images (e.g., HAM10000 [77]). Each image category has 5 datasets, and we  
 126 report their average performance in Figure 2 (see Table 9 in the Appendix C.1 for full results).

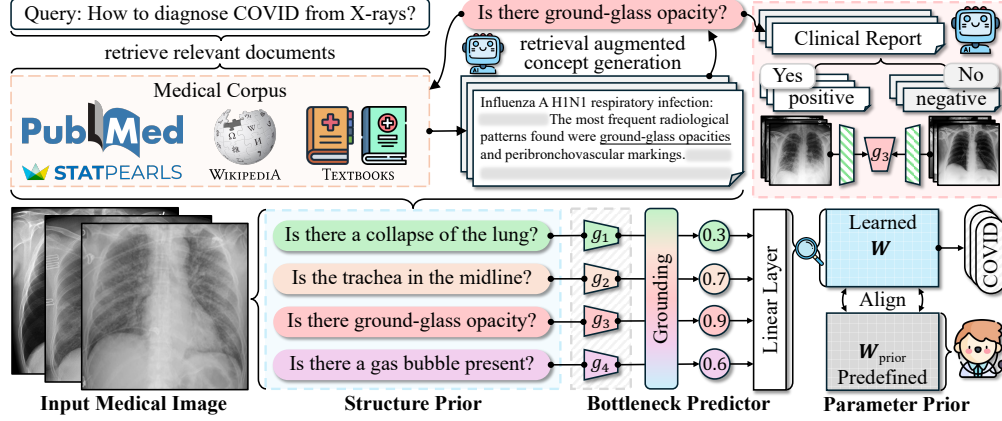


Figure 3: Overview of **Knowledge-enhanced Bottlenecks (KnoBo)** for medical image classification, comprising three main components: (1) **Structure Prior** (Sec 4.2) constructs the trustworthy knowledge bottleneck by leveraging medical documents; (2) **Bottleneck Predictor** (Sec 4.3) grounds the images onto concepts which are used as input for the linear layer and ; (3) **Parameter Prior** (Sec 4.4) constrains the learning of linear layer with parameters predefined by doctors or LLMs.

Figure 2 (left) shows vision backbones have effective priors for natural images, with ViT notably outperforming pixel by 14.7%. However, pixel features surpass those extracted by vision backbones for specialized domains such as X-ray and skin lesion images. This underscores these deep networks’ lack of image priors appropriate for these domains, which can hamper model learning and hurt generalizability. Without guidance from appropriate priors, models can overly rely on data, risking catastrophic failures. We aim to overcome this by injecting additional priors into models.

## 4 Knowledge-enhanced Bottlenecks

In this section, we present **Knowledge-enhanced Bottlenecks (KnoBo)**, a class of CBMs that incorporate knowledge priors that address the failures we identified in Section 3. Figure 3 presents an overview of our method, from left to right, we optimize three terms: (1) **Structure Prior** (Sec 4.2) induces bottleneck structures from medical corpus to incorporate human knowledge as concepts, (2) **Bottleneck Predictor** (Sec 4.3) projects input image onto bottleneck concepts and then feed concept predictions into the linear layer for label prediction, and (3) **Parameter Prior** (Sec 4.4) aligns the learned parameters with known associative information to further enhance priors.

### 4.1 Problem Formulation

**Preliminary on Concept Bottleneck Model.** Given a bottleneck  $C$  with  $N_C$  concepts, CBMs optimize two functions for predictions:  $\hat{y} = f(\mathcal{G}(x))$ , where  $\mathcal{G} : \mathbb{R}^d \rightarrow \mathbb{R}^{N_C}$  maps image features into concept space, and  $f : \mathbb{R}^{N_C} \rightarrow \mathcal{Y}$  uses concept predictions for final label predictions.

**Formulation.** Our goal is to incorporate priors over  $C$ , the concept structure, into the learning of the joint probability  $\sum_{(I,y) \in \mathcal{D}} \log P(y, C, \theta | I)$ , which can be decomposed into three factors:

$$\log P(y, C, \theta | I) = \underbrace{\log P(y | I, C, \theta)}_{\text{bottleneck predictor}} + \underbrace{\log P(C)}_{\text{structure prior}} + \underbrace{\log P(\theta)}_{\text{parameter prior}} \quad (1)$$

where we assume the priors over structure  $C$  and parameters  $\theta$  are independent. The **structure prior**  $P(C)$  (Sec 4.2) is formulated as the construction of a bottleneck with  $N_C$  concepts,  $C = \{c_1, c_2, \dots, c_{N_C}\}$ , derived from a background corpus  $\mathcal{B}$ . Each concept is a factor that humans will use when solving the same task. The **bottleneck predictor**  $P(y | I, C, \theta)$  (Sec 4.3) is a concept bottleneck model that predicts the label conditioned on the input image, bottleneck, and learned parameters. The bottleneck predictor is inherently interpretable, and each parameter in  $\theta$  has semantics, denoting the association between concepts and labels. The **parameter prior**  $P(\theta)$  (Sec 4.4) regularizes the learning of model parameters  $\theta$  with information derived from human knowledge. Jointly optimizing over structure and model parameters is intractable, so we first select a high-quality concept space and then optimize the parameters of the bottleneck jointly with the parameter prior.

## 4.2 Structural Prior

Given a background corpus  $\mathcal{B}$  that spans various documents, we aim to identify a bottleneck structure containing concepts beneficial for classifying labels  $y \in \mathcal{Y}$ . As outlined in Algorithm 1, we use the class names  $\mathcal{Y}$  as initial queries to retrieve relevant documents  $\mathcal{B}' \subset \mathcal{B}$ . Large Language Models (LLMs) are then prompted to generate concepts using these retrieved documents as context:  $C' = \text{LLM}(\mathcal{B}')$ . These newly generated concepts are added to the bottleneck and used as new queries to retrieve additional documents. This iterative process continues to expand the bottleneck until a predetermined number of concepts  $N_C$  is reached. Such concept structures have high likelihood under the language model, conditioned on the background corpus, and the language model probability serves as an implicit prior.

**Algorithm 1** Retrieval Augmented Iterative Concept Bottleneck Generation

---

```

 $\mathcal{Y}$ , set of target class names
 $\mathcal{B}$ , set of background documents
 $\mathcal{Q} \leftarrow \mathcal{Y}$ , class names as initial queries
 $C \leftarrow []$ , concepts in the bottleneck
while  $|C| < N_C$  do
   $\mathcal{Q}' \leftarrow []$ , set of new queries
  for  $q$  in  $\mathcal{Q}$  do
     $\mathcal{B}' = \text{Retrieve}(\mathcal{B}, q)$ 
     $C' = \text{LLM}(\mathcal{B}')$ 
     $C \leftarrow C + C'$ ,  $\mathcal{Q}' \leftarrow \mathcal{Q}' + C'$ 
  end for
   $\mathcal{Q} \leftarrow \mathcal{Q}'$  /* update queries */
end while

```

---

## 4.3 Bottleneck Predictor

With the structure prior from the background corpus, we optimize (1) the grounding function  $\mathcal{G} : \mathbb{R}^d \rightarrow \mathbb{R}^{N_C}$ , which maps the input image to the concept space, and (2) a linear layer  $f : \mathbb{R}^{N_C} \rightarrow \mathcal{Y}$  that projects concept predictions onto labels. In practice, we implement  $\mathcal{G}$  as a set of grounding functions:  $\mathcal{G} = \{g_c\}_{c \in C}$  where each  $g_c$  predicts the probability of an image  $I$  having the concept  $c$ ,  $P(c|I) = g_c(\mathbf{x})$ , and  $\mathbf{x} \in \mathbb{R}^d$  is the image feature. Specifically, we derive training examples for grounding functions from a pretraining dataset of image-text pairs. We use the language model to estimate the presence of a concept in the image based on the information in the accompanying text.

**Concept Grounding.** Suppose we have a pretraining dataset  $\mathcal{D}_{\text{pre}}$  of image-text pairs  $\{(I, t)\}$ , where  $t$  is a textual description (such as a clinical report) of the image. Based on  $t$ , we can infer if a concept  $c$  is present in the image. This can be automated by prompting a large language model to generate a response indicating whether the text implies the concept. This way, we label our pretraining data as positive and negative examples for each concept  $c$ , which can be used to train its grounding function. With those annotated training examples, we implement each grounding function as a binary logistic regression classifier:  $g_c(\mathbf{x}) = \sigma(\mathbf{x} \cdot \mathbf{W}_c^\top)$ , where  $\mathbf{W}_c \in \mathbb{R}^d$  is the weights of grounding function and  $\sigma$  is the sigmoid activation. Finally, we form a collection of grounding functions  $\mathcal{G} = \{g_c\}_{c \in C}$  to map an image feature  $\mathbf{x}$  into  $N_C$  probabilities over all bottleneck concepts, with  $\mathcal{G}(\mathbf{x}) \in \mathbb{R}^{N_C}$ .

**Linear Layer.** Using concept probabilities  $\mathcal{G}(\mathbf{x})$  as input, we train a simple linear function  $f$  to make the final label prediction:  $\hat{y} = f(\mathcal{G}(\mathbf{x})) = \mathcal{G}(\mathbf{x}) \cdot \mathbf{W}^\top$ , where  $\mathbf{W} \in \mathbb{R}^{N \times N_C}$  is the linear weight matrix, with  $N$  the number of classes and  $N_C$  the number of concepts.

## 4.4 Parameter Prior

The bottleneck predictor is inherently interpretable because the parameters of the linear layer encode the affinity between labels and concepts. Therefore, we can guide the parameters based on prior knowledge, i.e., if the label  $y$  is positively related to concept  $c$  based on background knowledge, the weight  $w_{y,c} \in \mathbf{W}$  should be high. We hope the learned parameters do not deviate too much from this assumption, otherwise, the model may capture spurious correlations in the data.

To enforce this, we let language models define a weight matrix of priors  $\mathbf{W}_{\text{prior}} \in \mathbb{R}^{N \times N_C}$ , with each element  $w_{y,c} \in \{-1, +1\}$  indicating the sign of a preferred correlation between the label  $y$  and concept  $c$ . The prior loss is calculated as the L1 distance between  $\mathbf{W}$  and  $\mathbf{W}_{\text{prior}}$ :

$$\mathcal{L}_{\text{prior}} = \frac{1}{N \cdot N_C} \cdot \|\tanh(\mathbf{W}) - \mathbf{W}_{\text{prior}}\|_1 \quad (2)$$

in which we apply tanh activation on  $\mathbf{W}$  to scale the linear weights to  $(-1, 1)$ , matching the scale of the weights in the prior matrix. This adjustment aligns the model's parameters with the expected sign of the correlations based on prior knowledge. The final loss function to train the linear layer is the sum of the cross-entropy loss and the prior loss:  $\mathcal{L} = \mathcal{L}_{\text{CE}} + \mathcal{L}_{\text{prior}}$ .

In summary, we search for a structure  $C$  that is consistent with prior knowledge from a background corpus  $\mathcal{B}$  to serve as the bottleneck for the predictor  $P(y|I, C, \theta)$ . The parameters  $\theta$  are aligned with the predefined correlations between labels and concepts identified by language models.

## 5 Experimental Setup

This section introduces (1) the confounded and unconfounded medical datasets to evaluate the robustness of our knowledge-enhanced bottlenecks (Sec 5.1), (2) the black-box and interpretable baselines for comparison (Sec 5.2), and (3) the implementation details of our method (Sec 5.3).

### 5.1 Datasets

We evaluate on two groups of datasets for each modality: (1) the **confounded datasets**, which aim to assess the **robustness** of models by creating splits with spurious correlations; (2) the **unconfounded datasets** are randomly split to measure the models’ **performance** in natural settings.

**Confounded Datasets.** As illustrated on the left of Figure 1, we formulate the confounded datasets as binary classification tasks, where each class is confounded with one factor. The confounding combinations are reversed for in-domain (train and validation) and out-of-domain (test) splits.

The confounded datasets of **chest X-ray** are constructed from NIH-CXR [83] and CheXpert [35] with their provided attributes: (1) **NIH-sex** uses sex (male, female) as the confounding factor; (2) **NIH-age** confounds the data with age (young, old); (3) **NIH-pos** analyzes the patient’s position (standing, lying down) during X-ray examinations; (4) **CheXpert-race** splits the data based on patient’s race (white, black or African American); (5) **NIH-CheXpert** confounds X-rays across datasets (NIH, CheXpert).

The confounded datasets of **skin lesion** are derived from the International Skin Imaging Collaboration (ISIC): (1) **ISIC-sex** and (2) **ISIC-age** are set up similarly to the X-ray datasets mentioned previously; (3) **ISIC-site** studies lesions developed on different sites of the body (head, extremities); (4) **ISIC-color** evaluates examples with different skin colors (light, dark); and (5) **ISIC-hospital** uses instances sampled from hospitals in different cities (Barcelona, Vienna).

**Unconfounded datasets.** We evaluate 10 datasets with random splits, 5 for each modality. *X-ray*: **Pneumonia** [39], **COVID-QU** [9], **NIH-CXR** [83], **Open-i** [16], and **VinDr-CXR** [58]. *Skin Lesion*: **HAM10000** [77], **BCN20000** [14], **PAD-UFES-20** [62], **Melanoma** [36], and **UWaterloo** [45].

All datasets are split into train/validation/test and ensure the validation and test set are balanced across classes. Detailed statistics and additional information on each dataset are provided in Appendix A.

**Pretraining Datasets.** The training of vision backbones and concept grounding functions utilizes datasets with image-text pairs. For X-rays, we choose MIMIC-CXR [37], which contains 377,110 X-ray images with accompanying clinical reports. Since there is no existing text-annotated dataset for skin lesion images, we employ GPT-4V [61] to generate captions (see examples in Figure 9) for a subset of 56,590 images from ISIC, without overlap of the confounded and unconfounded datasets.

### 5.2 Baselines

We compare KnoBo against both black-box models and interpretable concept bottleneck models.

**Black-box Models.** We include two end-to-end fine-tuning baselines: (1) **ViT-L/14** [17] and (2) **DenseNet121** [32], both pretrained on the pretraining datasets mentioned earlier. Additionally, (3) **Linear Probe** extracts visual features with the frozen ViT-L/14 encoder and learns a linear layer for classification. (4) **Language-shaped Learning (LSL)** [56] aims to disentangle the impact of knowledge and interpretable structure. Inspired by LSL via captioning, we finetune a ViT-L/14 with the same data used for concept grounding functions and apply a linear layer (see Appendix B.2).

**Concept Bottleneck Models.** (1) **Post-hoc CBM (PCBM-h)** [91] ensembles concept bottleneck models with black-box residual predictors. We let PCBM-h use the same bottlenecks as our KnoBo method; (2) **LaBo** [90] applies language models to generate concepts, followed by the submodular selection to identify a subset that enhances performance. Following their original settings, PCBM-h and LaBo use CLIP (fine-tuned on medical pretraining datasets) to align concepts with images.

Method	NIH-sex			NIH-age			NIH-pos			CheXpert-race			NIH-CheXpert		
	ID	OOD	Avg	ID	OOD	Avg	ID	OOD	Avg	ID	OOD	Avg	ID	OOD	Avg
ViT-L/14	<b>97.0</b>	30.9	64.0	<b>97.4</b>	3.2	50.3	<b>99.7</b>	2.7	51.2	<b>89.4</b>	48.2	68.8	<b>99.9</b>	0.1	50.0
DenseNet	91.4	32.1	61.8	90.6	15.6	53.1	<u>99.3</u>	1.0	50.2	85.0	55.4	70.2	<b>99.9</b>	0.2	50.1
Linear Probe	<u>94.2</u>	<u>46.7</u>	<u>70.5</u>	<u>95.0</u>	11.4	53.2	<u>99.3</u>	17.0	58.2	87.8	71.4	79.6	<u>99.6</u>	6.8	53.2
LSL	84.0	<u>74.3</u>	<u>79.2</u>	79.8	<b>53.8</b>	<b>66.8</b>	95.3	<u>39.0</u>	<u>67.2</u>	80.4	<u>76.4</u>	78.4	95.0	<u>31.8</u>	<u>63.4</u>
PCBM-h	94.2	45.6	69.9	95.0	10.8	52.9	<u>99.3</u>	17.0	58.2	88.0	71.4	79.7	<u>99.6</u>	8.2	53.9
LaBo	91.4	51.3	71.4	92.8	14.4	53.6	98.0	24.3	61.2	86.8	69.2	78.0	98.4	14.9	56.7
KnoBo (ours)	88.6	<b>78.6</b>	<b>83.6</b>	88.8	<u>38.8</u>	<u>63.8</u>	95.7	<b>45.3</b>	<b>70.5</b>	84.0	<b>79.0</b>	<b>81.5</b>	91.6	<b>52.3</b>	<b>72.0</b>

Method	ISIC-sex			ISIC-age			ISIC-site			ISIC-color			ISIC-hospital		
	ID	OOD	Avg	ID	OOD	Avg	ID	OOD	Avg	ID	OOD	Avg	ID	OOD	Avg
ViT-L/14	<b>92.0</b>	69.0	80.5	<b>95.0</b>	61.3	78.2	<b>94.8</b>	38.3	66.6	<b>96.9</b>	59.2	78.1	99.2	10.0	54.6
DenseNet	85.3	76.0	80.7	<u>93.7</u>	61.3	77.5	81.7	54.5	68.1	<u>93.9</u>	44.6	69.2	98.4	15.1	56.8
Linear Probe	86.0	69.7	77.8	<u>92.7</u>	60.7	76.7	<u>90.2</u>	37.2	63.7	90.8	65.8	78.3	<b>100.0</b>	27.1	63.6
LSL	82.7	<u>78.3</u>	<u>80.5</u>	90.3	<u>66.0</u>	<u>78.2</u>	84.3	<u>50.2</u>	<u>67.3</u>	87.3	73.1	80.2	<u>99.6</u>	<u>27.9</u>	<u>63.8</u>
PCBM-h	<u>86.7</u>	69.0	77.8	93.0	59.3	76.2	90.0	38.5	64.3	91.2	66.5	78.9	<b>100.0</b>	26.8	63.4
LaBo	83.0	69.3	76.2	91.3	61.0	76.2	88.0	39.3	63.7	86.9	<b>78.9</b>	<b>82.9</b>	<b>100.0</b>	8.6	54.3
KnoBo (ours)	84.0	<b>79.7</b>	<b>81.8</b>	88.0	<b>67.7</b>	<b>77.8</b>	80.7	<b>58.8</b>	<b>69.8</b>	89.2	<u>75.8</u>	<u>82.5</u>	88.2	<b>77.5</b>	<b>82.9</b>

Table 1: Results on 10 **confounded datasets** of two modalities (top-5 are X-ray and bottom-5 are skin lesion). We report in-domain (ID), out-of-domain (OOD), and average of ID and OOD (Avg) accuracy. The best score of each column is **bold**, and the second best is underlined.

252 All baselines use backbones trained on the same pretraining data as our method to ensure a fair  
253 comparison. Appendix B.2 provides additional details about the baselines.

254 **Evaluation Metrics.** We use accuracy as the metric since all evaluated datasets are single-label  
255 classification tasks with balanced validation and test sets. For confounded datasets, we report in-  
256 domain (ID, validation), out-of-domain (OOD, test), and domain-average (mean of ID and OOD)  
257 accuracies, along with domain gaps ( $\Delta = |\text{ID} - \text{OOD}|$ ), where a lower  $\Delta$  indicates better robustness.  
258 For unconfounded datasets, we report test accuracy. A robust and performant model must achieve  
259 a good compromise between confounded and unconfounded datasets. For all the baselines and our  
260 KnoBo method, the checkpoints with the highest validation accuracy are evaluated on the test set.

### 261 5.3 Implementation Details

262 **Pretraining of Medical CLIP.** We fine-tune OpenCLIP [34] (ViT-L/14 pretrained on LAION-2B  
263 [73]) on the pretraining medical data for each modality. Unlike previous work [18, 85, 92] that  
264 directly pairs medical images with sentences from clinical reports, we preprocess the reports by  
265 employing GPT-4 [1] to extract short phrases. Our CLIP models perform the best for both X-ray and  
266 skin lesion datasets in zero-shot and linear probing, as shown in Table 7 in the Appendix.

267 **Medical Corpus.** We download 5.5 million articles from PubMed and segment them into 156.9  
268 million snippets to serve as documents for retrieval. Alternatively, we take the medical corpus  
269 organized by MEDRAG [88], including documents from Wikipedia, StatPearls, and medical textbooks.  
270 We employ BM25 [66] as the ranking function for document retrieval.

271 **KnoBo Details.** We select GPT-4 (gpt-4-0613) as the underlying LLM for retrieval-augmented  
272 concept generation (Sec 4.2). For training concept grounding functions (Sec 4.3), we opt for Flan-T5-  
273 XXL [10] to annotate clinical reports for each concept, considering cost-efficiency. Unless otherwise  
274 specified, KnoBo uses bottlenecks constructed from PubMed, each containing 150 concepts. Figure 5  
275 shows our prompt, and during concept generation, we apply several heuristic filters (Appendix B.3).

## 276 6 Results

277 In this section, we discuss KnoBo’s performance on confounded and unconfounded medical image  
278 datasets (Sec 6.1) and analyze different knowledge resources and our model design (Sec 6.2).

Method	Chest X-ray Datasets						Skin Lesion Datasets					
	ID	OOD	$\Delta \downarrow$	Avg	Unconfd	Overall	ID	OOD	$\Delta \downarrow$	Avg	Unconfd	Overall
ViT-L/14	<b>96.7</b>	17.0	79.7	56.8	70.2	63.5	<b>95.6</b>	47.6	48.0	71.6	<b>84.3</b>	77.9
DenseNet	93.2	20.9	72.4	57.1	66.0	61.5	90.6	50.3	40.3	70.4	71.0	70.7
Linear Probe	95.2	30.7	64.5	62.9	73.8	68.4	91.9	52.1	39.8	72.0	82.8	77.4
LSL	86.9	55.1	31.8	71.0	67.0	69.0	88.9	59.1	29.8	74.0	77.2	75.6
PCBM-h	95.2	30.6	64.6	62.9	<b>74.7</b>	68.8	92.2	52.0	40.1	72.1	81.7	76.9
LaBo	93.5	34.8	58.7	64.2	72.1	68.1	89.9	51.4	38.4	70.6	80.0	75.3
KnoBo (ours)	89.7	<b>58.8</b>	<b>30.9</b>	<b>74.3</b>	73.1	<b>73.7</b>	86.0	<b>70.5</b>	<b>14.1</b>	<b>78.3</b>	78.1	<b>78.2</b>

Table 2: Averaged results across all datasets, including in-domain (ID), out-of-domain (OOD), domain-gap ( $\Delta$ , lower is better), and mean of ID and OOD (Avg) accuracy for confounded datasets. For unconfounded datasets (Unconfd), we report test accuracy. Overall performance is calculated as the mean of the Avg and Unconfd, the overall tradeoff between data conditions.

Knowledge Source	Chest X-ray Datasets				Skin Lesion Datasets			
	Confid	Unconfd	Overall	Diversity	Confid	Unconfd	Overall	Diversity
PROMPT	72.9	72.8	72.9	0.542	<b>78.4</b>	77.0	77.7	0.332
TEXTBOOKS	72.0	72.9	72.4	0.585	77.5	78.3	77.9	0.350
WIKIPEDIA	72.8	72.7	72.8	0.542	77.6	77.9	77.8	0.356
STATPEARLS	73.4	72.0	72.7	0.598	77.1	<b>79.1</b>	78.1	<b>0.379</b>
PUBMED	<b>74.3</b>	<b>73.1</b>	<b>73.7</b>	<b>0.619</b>	78.3	78.1	<b>78.2</b>	0.341

Table 3: Comparison of concept bottlenecks built from different knowledge sources. PROMPT is our baseline without retrieving documents for concept generation. We report the accuracy of confounded (Confid, average over ID and OOD), unconfounded (Unconfd) datasets, and the overall performance of all datasets. Diversity measures the difference between the concepts in a bottleneck.

## 6.1 Main Results

**KnoBo is more robust to domain shifts.** Table 1 shows the results on 10 confounded datasets of X-ray and skin lesions. Black-box models excel at in-domain (ID) data but drop significantly on out-of-domain (OOD) data, especially in datasets confounded by hospitals/resources (NIH-CheXpert and ISIC-hospital), which can be common when collecting medical datasets [12, 81]. KnoBo outperforms baselines in OOD and domain-average accuracy by large margins, ranking top-1 in eight datasets and second-best in the other two. End-to-end models (ViT-L/14, DenseNet) exhibit larger domain gaps than linear probes, as they have more parameters to optimize performance on in-domain data and capture spurious correlations. Shaping the visual representations with knowledge (LSL) improves robustness but underperforms KnoBo, with lower ID, OOD, and average performance across most datasets. PCBM-h combines interpretable and black-box predictions but exhibits behaviors similar to black-box models with severe drops across domains. Unlike KnoBo, which uses medical documents to create one global bottleneck for each modality, LaBo builds a bottleneck for each dataset using the in-domain data, which can be biased and affected by confounding factors, and so performs more poorly. In summary, KnoBo mitigates the catastrophic failures in domain shifts encountered by black-box models and is more robust against various confounding factors across modalities.

**KnoBo performs the best across confounded and unconfounded data.** Table 2 illustrates the performance averaged across confounded and unconfounded datasets. For both types of medical images, KnoBo achieves the best out-of-domain (OOD) and domain-average performance (Avg) with minimal domain gaps ( $\Delta$ ), outperforming the strongest end-to-end baseline (ViT-L/14) by 41.8% (X-ray) and 22.9% (skin lesion) in OOD accuracy. KnoBo achieves competitive performance for unconfounded X-ray datasets, trailing the best-performing black-box model (Linear Probe) by only 0.7%. While KnoBo is less competitive on skin lesion datasets due to the lack of large-scale pretraining data for accurate concept grounding, it still maintains performance comparable to the baselines. By calculating the mean accuracy across both confounded and unconfounded datasets, KnoBo ranks top across all models, confirming that our knowledge-enhanced, interpretable approach is a promising direction for building more robust and performant systems for medical imaging.



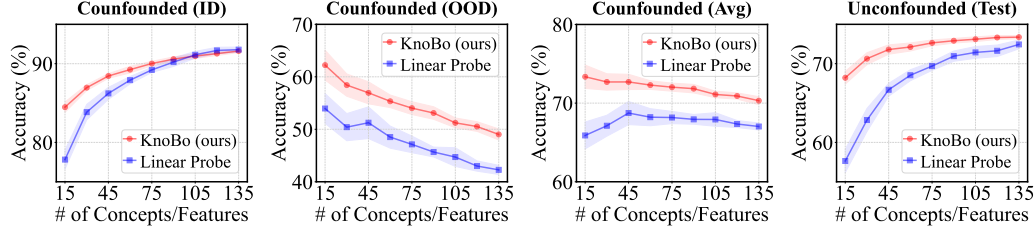


Figure 4: Ablation of **bottleneck sizes** on X-ray datasets. The x-axis is the number of randomly selected concepts (KnoBo) or visual features (Linear Probe).

Method	Chest X-ray Datasets						Skin Lesion Datasets					
	ID	OOD	$\Delta \downarrow$	Avg	Unconfd	Overall	ID	OOD	$\Delta \downarrow$	Avg	Unconfd	Overall
KnoBo	89.7	<b>58.8</b>	<b>30.9</b>	<b>74.3</b>	73.1	<b>73.7</b>	86.0	<b>70.5</b>	14.1	<b>78.3</b>	78.1	<b>78.2</b>
w/o $\mathcal{G}$	87.8	51.5	36.3	69.6	70.1	69.9	83.7	69.4	<b>11.5</b>	76.6	70.2	73.4
w/o $\mathcal{L}_{\text{prior}}$	<b>91.6</b>	48.1	43.5	69.8	<b>73.6</b>	71.7	<b>86.5</b>	69.1	16.6	77.8	<b>78.4</b>	78.1

Table 4: Ablation studies on concept grounding ( $\mathcal{G}$ ; Sec 4.3) and parameter prior ( $\mathcal{L}_{\text{prior}}$ ; Sec 4.4).

## 6.2 Analysis

In this section, we compare the bottlenecks constructed from different knowledge resources. We evaluate the impact of each component of KnoBo on the final performance, including bottleneck size, concept grounding function, and parameter prior. Additional analyses are available in Appendix C.

**Knowledge Sources.** Besides the empirical results on confounded and unconfounded datasets, we measure the diversity of bottleneck  $C$  as  $\text{Diversity}(C) = \frac{1}{|C|^2 - |C|} \sum_{c_i \in C} \sum_{c_j \in C, i \neq j} (1 - \text{sim}(c_i, c_j))$ , where the  $\text{sim}(\cdot)$  is the cosine similarity of concept features encoded by sentence transformer [65]. The **Diversity** computes the distance between each concept and every other concept in the bottleneck. Table 3 compares different knowledge sources. The retrieval-augmented bottlenecks perform better than those generated by prompting, especially for skin lesions, where more specific knowledge is required because prompting lacks diversity. Across both modalities, PubMed is the best overall, performing better for the X-ray modality than other knowledge sources and among the best for skin lesion modalities. In evaluations by two medical students, information from all knowledge sources is rated as highly relevant and groundable (see Appendix C.4). Moreover, shown in Table 12, our retrieval-augmented concepts are attributable, which allows doctors to verify the source of knowledge.

**Bottleneck Size.** Figure 4 compares KnoBo and linear probes while varying the number of concepts/features. KnoBo consistently outperforms linear probes across all metrics when given the same quota of features, and KnoBo can obtain good performance with fewer features. This demonstrates that interpretable concept scores have more effective priors than black-box visual features.

**Ablations.** Table 4 summarizes experiments ablating major components of our approach. Row 2 shows the performance of using dot-products from prompted CLIP models as concepts, which markedly reduces performance. This shows the importance of knowledge grounding in ensuring KnoBo’s effectiveness. However, this step can be simplified as more advanced medical foundation models are available. Row 3 shows performance omitting the parameter prior. It is an important mechanism for constraining the final phase of learning, resulting in consistent OOD improvements.

## 7 Conclusion and Limitation

In this paper, we analyze domain-shift problems in medical image analysis and identify a missing medical deep image prior as a main contributor of poor performance. To address this, we introduce knowledge-enhanced bottlenecks (KnoBo) to integrate knowledge priors from medical documents. Across two medical image modalities under various domain shifts, KnoBo significantly improves robustness. KnoBo assumes the availability of medical multimodal datasets limiting applications to rare conditions. While our work improves robustness, medical experts do not fail in these ways and they should be used to conjunction with models.

## References

- [1] J. Achiam, S. Adler, S. Agarwal, L. Ahmad, I. Akkaya, F. L. Aleman, D. Almeida, J. Altenschmidt, S. Altman, S. Anadkat, et al. Gpt-4 technical report. *arXiv preprint arXiv:2303.08774*, 2023.
- [2] M. Arjovsky, L. Bottou, I. Gulrajani, and D. Lopez-Paz. Invariant risk minimization. *arXiv preprint arXiv:1907.02893*, 2019.
- [3] A. J. Barnett, F. R. Schwartz, C. Tao, C. Chen, Y. Ren, J. Y. Lo, and C. Rudin. A case-based interpretable deep learning model for classification of mass lesions in digital mammography. *Nature Machine Intelligence*, 3(12):1061–1070, 2021.
- [4] P. J. Bevan and A. Atapour-Abarghouei. Detecting melanoma fairly: Skin tone detection and debiasing for skin lesion classification. In *MICCAI Workshop on Domain Adaptation and Representation Transfer*, pages 1–11. Springer, 2022.
- [5] R. Bommasani, D. A. Hudson, E. Adeli, R. Altman, S. Arora, S. von Arx, M. S. Bernstein, J. Bohg, A. Bosselut, E. Brunskill, et al. On the opportunities and risks of foundation models. *arXiv preprint arXiv:2108.07258*, 2021.
- [6] H. P. Boshuizen and H. G. Schmidt. On the role of biomedical knowledge in clinical reasoning by experts, intermediates and novices. *Cognitive science*, 16(2):153–184, 1992.
- [7] L. Bossard, M. Guillaumin, and L. Van Gool. Food-101—mining discriminative components with random forests. In *Computer Vision—ECCV 2014: 13th European Conference, Zurich, Switzerland, September 6–12, 2014, Proceedings, Part VI 13*, pages 446–461. Springer, 2014.
- [8] C. Chen, O. Li, D. Tao, A. Barnett, C. Rudin, and J. K. Su. This looks like that: deep learning for interpretable image recognition. *Advances in neural information processing systems*, 32, 2019.
- [9] M. E. Chowdhury, T. Rahman, A. Khandakar, R. Mazhar, M. A. Kadir, Z. B. Mahbub, K. R. Islam, M. S. Khan, A. Iqbal, N. Al Emadi, et al. Can ai help in screening viral and covid-19 pneumonia? *Ieee Access*, 8:132665–132676, 2020.
- [10] H. W. Chung, L. Hou, S. Longpre, B. Zoph, Y. Tay, W. Fedus, Y. Li, X. Wang, M. Dehghani, S. Brahma, et al. Scaling instruction-finetuned language models. *Journal of Machine Learning Research*, 25(70):1–53, 2024.
- [11] A. Coates, A. Ng, and H. Lee. An analysis of single-layer networks in unsupervised feature learning. In *Proceedings of the fourteenth international conference on artificial intelligence and statistics*, pages 215–223. JMLR Workshop and Conference Proceedings, 2011.
- [12] J. P. Cohen, P. Morrison, and L. Dao. Covid-19 image data collection. *arXiv preprint arXiv:2003.11597*, 2020.
- [13] J. P. Cohen, J. D. Viviano, P. Bertin, P. Morrison, P. Torabian, M. Guarrera, M. P. Lungren, A. Chaudhari, R. Brooks, M. Hashir, and H. Bertrand. TorchXRyVision: A library of chest X-ray datasets and models. In *Medical Imaging with Deep Learning*, 2022. URL <https://github.com/mlmed/torchxrayvision>.
- [14] M. Combalia, N. C. Codella, V. Rotemberg, B. Helba, V. Vilaplana, O. Reiter, C. Carrera, A. Barreiro, A. C. Halpern, S. Puig, et al. Bcn20000: Dermoscopic lesions in the wild. *arXiv preprint arXiv:1908.02288*, 2019.
- [15] A. J. DeGrave, J. D. Janizek, and S.-I. Lee. Ai for radiographic covid-19 detection selects shortcuts over signal. *Nature Machine Intelligence*, 3(7):610–619, 2021.
- [16] D. Demner-Fushman, S. Antani, M. Simpson, and G. R. Thoma. Design and development of a multimodal biomedical information retrieval system. *Journal of Computing Science and Engineering*, 6(2):168–177, 2012.

- [17] A. Dosovitskiy, L. Beyer, A. Kolesnikov, D. Weissenborn, X. Zhai, T. Unterthiner, M. Dehghani, M. Minderer, G. Heigold, S. Gelly, et al. An image is worth 16x16 words: Transformers for image recognition at scale. *arXiv preprint arXiv:2010.11929*, 2020.
- [18] S. Eslami, G. de Melo, and C. Meinel. Does CLIP benefit visual question answering in the medical domain as much as it does in the general domain? *arXiv e-prints*, art. arXiv:2112.13906, Dec. 2021.
- [19] T. B. Fitzpatrick. The validity and practicality of sun-reactive skin types i through vi. *Archives of dermatology*, 124(6):869–871, 1988.
- [20] G. Frisoni, M. Mizutani, G. Moro, and L. Valgimigli. BioReader: a retrieval-enhanced text-to-text transformer for biomedical literature. In Y. Goldberg, Z. Kozareva, and Y. Zhang, editors, *Proceedings of the 2022 Conference on Empirical Methods in Natural Language Processing*, pages 5770–5793, Abu Dhabi, United Arab Emirates, Dec. 2022. Association for Computational Linguistics. doi: 10.18653/v1/2022.emnlp-main.390. URL <https://aclanthology.org/2022.emnlp-main.390>.
- [21] J. Futoma, M. Simons, T. Panch, F. Doshi-Velez, and L. A. Celi. The myth of generalisability in clinical research and machine learning in health care. *The Lancet Digital Health*, 2(9):e489–e492, 2020.
- [22] Y. Ganin, E. Ustinova, H. Ajakan, P. Germain, H. Larochelle, F. Laviolette, M. March, and V. Lempitsky. Domain-adversarial training of neural networks. *Journal of machine learning research*, 17(59):1–35, 2016.
- [23] Y. Gao, Y. Xiong, X. Gao, K. Jia, J. Pan, Y. Bi, Y. Dai, J. Sun, and H. Wang. Retrieval-augmented generation for large language models: A survey. *arXiv preprint arXiv:2312.10997*, 2023.
- [24] J. W. Gichoya, I. Banerjee, A. R. Bhimireddy, J. L. Burns, L. A. Celi, L.-C. Chen, R. Correa, N. Dullerud, M. Ghassemi, S.-C. Huang, et al. Ai recognition of patient race in medical imaging: a modelling study. *The Lancet Digital Health*, 4(6):e406–e414, 2022.
- [25] H. Guan and M. Liu. Domain adaptation for medical image analysis: a survey. *IEEE Transactions on Biomedical Engineering*, 69(3):1173–1185, 2021.
- [26] I. Gulrajani and D. Lopez-Paz. In search of lost domain generalization. *arXiv preprint arXiv:2007.01434*, 2020.
- [27] L. L. Guo, S. R. Pfohl, J. Fries, A. E. Johnson, J. Posada, C. Aftandilian, N. Shah, and L. Sung. Evaluation of domain generalization and adaptation on improving model robustness to temporal dataset shift in clinical medicine. *Scientific reports*, 12(1):2726, 2022.
- [28] K. He, X. Zhang, S. Ren, and J. Sun. Delving deep into rectifiers: Surpassing human-level performance on imagenet classification. In *Proceedings of the IEEE international conference on computer vision*, pages 1026–1034, 2015.
- [29] L. A. Hendricks, Z. Akata, M. Rohrbach, J. Donahue, B. Schiele, and T. Darrell. Generating visual explanations. In *Computer Vision—ECCV 2016: 14th European Conference, Amsterdam, The Netherlands, October 11–14, 2016, Proceedings, Part IV 14*, pages 3–19. Springer, 2016.
- [30] A. Holzinger, G. Langs, H. Denk, K. Zatloukal, and H. Müller. Causability and explainability of artificial intelligence in medicine. *Wiley Interdisciplinary Reviews: Data Mining and Knowledge Discovery*, 9(4):e1312, 2019.
- [31] Z. Hu, A. Iscen, C. Sun, Z. Wang, K.-W. Chang, Y. Sun, C. Schmid, D. A. Ross, and A. Fathi. Reveal: Retrieval-augmented visual-language pre-training with multi-source multimodal knowledge memory. In *Proceedings of the IEEE/CVF conference on computer vision and pattern recognition*, pages 23369–23379, 2023.
- [32] G. Huang, Z. Liu, L. Van Der Maaten, and K. Q. Weinberger. Densely connected convolutional networks. In *Proceedings of the IEEE conference on computer vision and pattern recognition*, pages 4700–4708, 2017.

- [33] B. Y. Idrissi, M. Arjovsky, M. Pezeshki, and D. Lopez-Paz. Simple data balancing achieves competitive worst-group-accuracy. In *Conference on Causal Learning and Reasoning*, pages 336–351. PMLR, 2022.
- [34] G. Ilharco, M. Wortsman, R. Wightman, C. Gordon, N. Carlini, R. Taori, A. Dave, V. Shankar, H. Namkoong, J. Miller, H. Hajishirzi, A. Farhadi, and L. Schmidt. Openclip, July 2021. URL <https://doi.org/10.5281/zenodo.5143773>. If you use this software, please cite it as below.
- [35] J. Irvin, P. Rajpurkar, M. Ko, Y. Yu, S. Ciurea-Ilcus, C. Chute, H. Marklund, B. Haghighi, R. Ball, K. Shpanskaya, et al. Chexpert: A large chest radiograph dataset with uncertainty labels and expert comparison. In *Proceedings of the AAAI conference on artificial intelligence*, volume 33, pages 590–597, 2019.
- [36] M. H. Javid. Melanoma skin cancer dataset of 10000 images, 2022. URL <https://www.kaggle.com/dsv/3376422>.
- [37] A. E. Johnson, T. J. Pollard, S. J. Berkowitz, N. R. Greenbaum, M. P. Lungren, C.-y. Deng, R. G. Mark, and S. Horng. Mimic-cxr, a de-identified publicly available database of chest radiographs with free-text reports. *Scientific data*, 6(1):317, 2019.
- [38] N. Kandpal, H. Deng, A. Roberts, E. Wallace, and C. Raffel. Large language models struggle to learn long-tail knowledge. In *International Conference on Machine Learning*, pages 15696–15707. PMLR, 2023.
- [39] D. S. Kermany, M. Goldbaum, W. Cai, C. C. Valentim, H. Liang, S. L. Baxter, A. McKeown, G. Yang, X. Wu, F. Yan, et al. Identifying medical diagnoses and treatable diseases by image-based deep learning. *cell*, 172(5):1122–1131, 2018.
- [40] P. Kirichenko, P. Izmailov, and A. G. Wilson. Last layer re-training is sufficient for robustness to spurious correlations. *arXiv preprint arXiv:2204.02937*, 2022.
- [41] P. W. Koh, T. Nguyen, Y. S. Tang, S. Mussmann, E. Pierson, B. Kim, and P. Liang. Concept bottleneck models. In *International conference on machine learning*, pages 5338–5348. PMLR, 2020.
- [42] P. W. Koh, S. Sagawa, H. Marklund, S. M. Xie, M. Zhang, A. Balsubramani, W. Hu, M. Yasunaga, R. L. Phillips, I. Gao, et al. Wilds: A benchmark of in-the-wild distribution shifts. In *International conference on machine learning*, pages 5637–5664. PMLR, 2021.
- [43] A. Krizhevsky, G. Hinton, et al. Learning multiple layers of features from tiny images, 2009.
- [44] D. Krueger, E. Caballero, J.-H. Jacobsen, A. Zhang, J. Binas, D. Zhang, R. Le Priol, and A. Courville. Out-of-distribution generalization via risk extrapolation (rex). In *International Conference on Machine Learning*, pages 5815–5826. PMLR, 2021.
- [45] V. I. Lab. University of waterloo skin cancer database, 2021. URL <https://uwaterloo.ca/vision-image-processing-lab/research-demos/skin-cancer-detection>.
- [46] A. J. Larrazabal, N. Nieto, V. Peterson, D. H. Milone, and E. Ferrante. Gender imbalance in medical imaging datasets produces biased classifiers for computer-aided diagnosis. *Proceedings of the National Academy of Sciences*, 117(23):12592–12594, 2020.
- [47] Y. Lee, A. S. Chen, F. Tajwar, A. Kumar, H. Yao, P. Liang, and C. Finn. Surgical fine-tuning improves adaptation to distribution shifts. *International Conference on Learning Representations*, 2023.
- [48] P. Lewis, E. Perez, A. Piktus, F. Petroni, V. Karpukhin, N. Goyal, H. Küttler, M. Lewis, W.-t. Yih, T. Rocktäschel, et al. Retrieval-augmented generation for knowledge-intensive nlp tasks. *Advances in Neural Information Processing Systems*, 33:9459–9474, 2020.
- [49] C. Li, C. Wong, S. Zhang, N. Usuyama, H. Liu, J. Yang, T. Naumann, H. Poon, and J. Gao. Llava-med: Training a large language-and-vision assistant for biomedicine in one day. *arXiv preprint arXiv:2306.00890*, 2023.

- [50] W. Lin and B. Byrne. Retrieval augmented visual question answering with outside knowledge. In Y. Goldberg, Z. Kozareva, and Y. Zhang, editors, *Proceedings of the 2022 Conference on Empirical Methods in Natural Language Processing*, pages 11238–11254, Abu Dhabi, United Arab Emirates, Dec. 2022. Association for Computational Linguistics. doi: 10.18653/v1/2022.emnlp-main.772. URL <https://aclanthology.org/2022.emnlp-main.772>.
- [51] Z. Liu, H. Mao, C.-Y. Wu, C. Feichtenhofer, T. Darrell, and S. Xie. A convnet for the 2020s. *Proceedings of the IEEE/CVF Conference on Computer Vision and Pattern Recognition (CVPR)*, 2022.
- [52] M. Luo, Y. Zeng, P. Banerjee, and C. Baral. Weakly-supervised visual-retriever-reader for knowledge-based question answering. In M.-F. Moens, X. Huang, L. Specia, and S. W.-t. Yih, editors, *Proceedings of the 2021 Conference on Empirical Methods in Natural Language Processing*, pages 6417–6431, Online and Punta Cana, Dominican Republic, Nov. 2021. Association for Computational Linguistics. doi: 10.18653/v1/2021.emnlp-main.517. URL <https://aclanthology.org/2021.emnlp-main.517>.
- [53] K. Marino, M. Rastegari, A. Farhadi, and R. Mottaghi. Ok-vqa: A visual question answering benchmark requiring external knowledge. In *Conference on Computer Vision and Pattern Recognition (CVPR)*, 2019.
- [54] D. McInerney, G. Young, J.-W. van de Meent, and B. Wallace. CHiLL: Zero-shot custom interpretable feature extraction from clinical notes with large language models. In H. Bouamor, J. Pino, and K. Bali, editors, *Findings of the Association for Computational Linguistics: EMNLP 2023*, pages 8477–8494, Singapore, Dec. 2023. Association for Computational Linguistics. doi: 10.18653/v1/2023.findings-emnlp.568. URL <https://aclanthology.org/2023.findings-emnlp.568>.
- [55] M. Moor, O. Banerjee, Z. S. H. Abad, H. M. Krumholz, J. Leskovec, E. J. Topol, and P. Rajpurkar. Foundation models for generalist medical artificial intelligence. *Nature*, 616(7956):259–265, 2023.
- [56] J. Mu, P. Liang, and N. Goodman. Shaping visual representations with language for few-shot classification. *arXiv preprint arXiv:1911.02683*, 2019.
- [57] K. Muandet, D. Balduzzi, and B. Schölkopf. Domain generalization via invariant feature representation. In *International conference on machine learning*, pages 10–18. PMLR, 2013.
- [58] H. Q. Nguyen, K. Lam, L. T. Le, H. H. Pham, D. Q. Tran, D. B. Nguyen, D. D. Le, C. M. Pham, H. T. T. Tong, D. H. Dinh, C. D. Do, L. T. Doan, C. N. Nguyen, B. T. Nguyen, Q. V. Nguyen, A. D. Hoang, H. N. Phan, A. T. Nguyen, P. H. Ho, D. T. Ngo, N. T. Nguyen, N. T. Nguyen, M. Dao, and V. Vu. Vindr-cxr: An open dataset of chest x-rays with radiologist’s annotations, 2020.
- [59] M.-E. Nilsback and A. Zisserman. Automated flower classification over a large number of classes. In *2008 Sixth Indian conference on computer vision, graphics & image processing*, pages 722–729. IEEE, 2008.
- [60] T. Oikarinen, S. Das, L. M. Nguyen, and T.-W. Weng. Label-free concept bottleneck models. *arXiv preprint arXiv:2304.06129*, 2023.
- [61] OpenAI. Gpt-4v(ision) technical work and authors., 2023. URL <https://cdn.openai.com/contributions/gpt-4v.pdf>.
- [62] A. G. Pacheco, G. R. Lima, A. S. Salomao, B. Krohling, I. P. Biral, G. G. de Angelo, F. C. Alves Jr, J. G. Esgario, A. C. Simora, P. B. Castro, et al. Pad-ufes-20: A skin lesion dataset composed of patient data and clinical images collected from smartphones. *Data in brief*, 32: 106221, 2020.
- [63] F. Qiao, L. Zhao, and X. Peng. Learning to learn single domain generalization. In *Proceedings of the IEEE/CVF conference on computer vision and pattern recognition*, pages 12556–12565, 2020.

- [64] A. Radford, J. W. Kim, C. Hallacy, A. Ramesh, G. Goh, S. Agarwal, G. Sastry, A. Askell, P. Mishkin, J. Clark, et al. Learning transferable visual models from natural language supervision. In *International conference on machine learning*, pages 8748–8763. PMLR, 2021.
- [65] N. Reimers and I. Gurevych. Sentence-bert: Sentence embeddings using siamese bert-networks. In *Proceedings of the 2019 Conference on Empirical Methods in Natural Language Processing*. Association for Computational Linguistics, 11 2019. URL <https://arxiv.org/abs/1908.10084>.
- [66] S. Robertson, H. Zaragoza, et al. The probabilistic relevance framework: Bm25 and beyond. *Foundations and Trends® in Information Retrieval*, 3(4):333–389, 2009.
- [67] E. Rosenfeld, P. Ravikumar, and A. Risteski. The risks of invariant risk minimization. *arXiv preprint arXiv:2010.05761*, 2020.
- [68] E. Rosenfeld, P. Ravikumar, and A. Risteski. Domain-adjusted regression or: Erm may already learn features sufficient for out-of-distribution generalization. *arXiv preprint arXiv:2202.06856*, 2022.
- [69] C. Rudin. Stop explaining black box machine learning models for high stakes decisions and use interpretable models instead. *Nature machine intelligence*, 1(5):206–215, 2019.
- [70] O. Russakovsky, J. Deng, H. Su, J. Krause, S. Satheesh, S. Ma, Z. Huang, A. Karpathy, A. Khosla, M. Bernstein, et al. Imagenet large scale visual recognition challenge. *International journal of computer vision*, 115:211–252, 2015.
- [71] S. Sagawa, P. W. Koh, T. B. Hashimoto, and P. Liang. Distributionally robust neural networks for group shifts: On the importance of regularization for worst-case generalization. *arXiv preprint arXiv:1911.08731*, 2019.
- [72] A. M. Saxe, P. W. Koh, Z. Chen, M. Bhand, B. Suresh, and A. Y. Ng. On random weights and unsupervised feature learning. In *ICML*, volume 2, page 6, 2011.
- [73] C. Schuhmann, R. Beaumont, R. Vencu, C. Gordon, R. Wightman, M. Cherti, T. Coombes, A. Katta, C. Mullis, M. Wortsman, et al. Laion-5b: An open large-scale dataset for training next generation image-text models. *Advances in Neural Information Processing Systems*, 35: 25278–25294, 2022.
- [74] D. Schwenk, A. Khandelwal, C. Clark, K. Marino, and R. Mottaghi. A-okvqa: A benchmark for visual question answering using world knowledge. *arXiv*, 2022.
- [75] R. R. Selvaraju, M. Cogswell, A. Das, R. Vedantam, D. Parikh, and D. Batra. Grad-cam: Visual explanations from deep networks via gradient-based localization. In *Proceedings of the IEEE international conference on computer vision*, pages 618–626, 2017.
- [76] K. Simonyan, A. Vedaldi, and A. Zisserman. Deep inside convolutional networks: Visualising image classification models and saliency maps. *arXiv preprint arXiv:1312.6034*, 2013.
- [77] P. Tschandl, C. Rosendahl, and H. Kittler. The ham10000 dataset, a large collection of multi-source dermatoscopic images of common pigmented skin lesions. *Scientific data*, 5(1):1–9, 2018.
- [78] D. Ulyanov, A. Vedaldi, and V. Lempitsky. Deep image prior. In *Proceedings of the IEEE conference on computer vision and pattern recognition*, pages 9446–9454, 2018.
- [79] A. Vellido. The importance of interpretability and visualization in machine learning for applications in medicine and health care. *Neural computing and applications*, 32(24):18069–18083, 2020.
- [80] R. Volpi, H. Namkoong, O. Sener, J. C. Duchi, V. Murino, and S. Savarese. Generalizing to unseen domains via adversarial data augmentation. *Advances in neural information processing systems*, 31, 2018.

- [81] L. Wang, Z. Q. Lin, and A. Wong. Covid-net: A tailored deep convolutional neural network design for detection of covid-19 cases from chest x-ray images. *Scientific reports*, 10(1):19549, 2020.
- [82] P. Wang, Q. Wu, C. Shen, A. v. d. Hengel, and A. Dick. Explicit knowledge-based reasoning for visual question answering. *arXiv preprint arXiv:1511.02570*, 2015.
- [83] X. Wang, Y. Peng, L. Lu, Z. Lu, M. Bagheri, and R. M. Summers. Chestx-ray8: Hospital-scale chest x-ray database and benchmarks on weakly-supervised classification and localization of common thorax diseases. In *Proceedings of the IEEE conference on computer vision and pattern recognition*, pages 2097–2106, 2017.
- [84] Y. Wang, X. Ma, and W. Chen. Augmenting black-box llms with medical textbooks for clinical question answering. *arXiv preprint arXiv:2309.02233*, 2023.
- [85] Z. Wang, Z. Wu, D. Agarwal, and J. Sun. MedCLIP: Contrastive learning from unpaired medical images and text. In Y. Goldberg, Z. Kozareva, and Y. Zhang, editors, *Proceedings of the 2022 Conference on Empirical Methods in Natural Language Processing*, pages 3876–3887, Abu Dhabi, United Arab Emirates, Dec. 2022. Association for Computational Linguistics. doi: 10.18653/v1/2022.emnlp-main.256. URL <https://aclanthology.org/2022.emnlp-main.256>.
- [86] K. Wantlin, C. Wu, S.-C. Huang, O. Banerjee, F. Dadabhoy, V. V. Mehta, R. W. Han, F. Cao, R. R. Narayan, E. Colak, et al. Benchmd: A benchmark for modality-agnostic learning on medical images and sensors. *arXiv preprint arXiv:2304.08486*, 2023.
- [87] Y. Wu, Y. Liu, Y. Yang, M. S. Yao, W. Yang, X. Shi, L. Yang, D. Li, Y. Liu, J. C. Gee, et al. A concept-based interpretable model for the diagnosis of choroid neoplasias using multimodal data. *arXiv preprint arXiv:2403.05606*, 2024.
- [88] G. Xiong, Q. Jin, Z. Lu, and A. Zhang. Benchmarking retrieval-augmented generation for medicine. *arXiv preprint arXiv:2402.13178*, 2024.
- [89] A. Yan, Y. Wang, Y. Zhong, Z. He, P. Karypis, Z. Wang, C. Dong, A. Gentili, C.-N. Hsu, J. Shang, et al. Robust and interpretable medical image classifiers via concept bottleneck models. *arXiv preprint arXiv:2310.03182*, 2023.
- [90] Y. Yang, A. Panagopoulou, S. Zhou, D. Jin, C. Callison-Burch, and M. Yatskar. Language in a bottle: Language model guided concept bottlenecks for interpretable image classification. In *Proceedings of the IEEE/CVF Conference on Computer Vision and Pattern Recognition*, pages 19187–19197, 2023.
- [91] M. Yuksekgonul, M. Wang, and J. Zou. Post-hoc concept bottleneck models. In *The Eleventh International Conference on Learning Representations*, 2023. URL <https://openreview.net/forum?id=nA5AZ8CEyow>.
- [92] S. Zhang, Y. Xu, N. Usuyama, H. Xu, J. Bagga, R. Tinn, S. Preston, R. Rao, M. Wei, N. Valluri, et al. Biomedclip: a multimodal biomedical foundation model pretrained from fifteen million scientific image-text pairs. *arXiv preprint arXiv:2303.00915*, 2023.
- [93] X. Zhang, P. Cui, R. Xu, L. Zhou, Y. He, and Z. Shen. Deep stable learning for out-of-distribution generalization. In *Proceedings of the IEEE/CVF Conference on Computer Vision and Pattern Recognition*, pages 5372–5382, 2021.
- [94] X. Zhang, C. Wu, Y. Zhang, W. Xie, and Y. Wang. Knowledge-enhanced visual-language pre-training on chest radiology images. *Nature Communications*, 14(1):4542, 2023.
- [95] B. Zhou, A. Khosla, A. Lapedriza, A. Oliva, and A. Torralba. Learning deep features for discriminative localization. In *Proceedings of the IEEE conference on computer vision and pattern recognition*, pages 2921–2929, 2016.
- [96] X. Zhou, Y. Lin, R. Pi, W. Zhang, R. Xu, P. Cui, and T. Zhang. Model agnostic sample reweighting for out-of-distribution learning. In *International Conference on Machine Learning*, pages 27203–27221. PMLR, 2022.

## 625 A Dataset

Dataset Name	Confounding Factor	n. of Class	Class Names	n. of Images		
				train	val	test
NIH-sex	sex	2	Atelectasis, Effusion	3000	500	1000
NIH-age	age	2	No finding, Has findings	3000	500	500
NIH-pos	position	2	Atelectasis, Effusion	3000	300	300
CheXpert-race	race	2	No finding, Has findings	4000	500	500
NIH-CheXpert	dataset	2	Atelectasis, Effusion	5000	1000	1000
Pneumonia [39]	-	2	Normal, Pneumonia	5216	16	624
COVID-QU [9]	-	4	COVID, Lung Opacity, Normal, Viral Pneumonia	16930	2115	2114
NIH-CXR [83]	-	6	Atelectasis, Cardiomegaly, Effusion Consolidation, Edema, Pneumonia	8066	1140	2317
Open-i [16]	-	3	Cardiomegaly, Lung Opacity, Normal	884	438	890
VinDr-CXR [58]	-	7	Aortic enlargement, Cardiomegaly, Pulmonary fibrosis, Lung Opacity, Pleural thickening, Nodule, Normal	1400	175	175

Table 5: Detailed statistics of the 10 Chest X-ray datasets evaluated in this work.

Dataset Name	Confounding Factor	n. of Class	Class Names	n. of Images		
				train	val	test
ISIC-sex	sex	2	Benign, Malignant	2400	300	300
ISIC-age	age	2	Benign, Malignant	2800	300	300
ISIC-site	body site	2	Benign, Malignant	2000	600	600
ISIC-color	skin color	2	Benign, Malignant	1800	260	260
ISIC-hospital	hospital	2	Benign, Malignant	2400	280	280
HAM10000 [77]	-	7	Actinic Keratoses, Basal Cell Carcinoma, Benign Keratosis-like Lesions, Dermatofibroma, Melanocytic Nevi, Melanoma, Vascular Lesions	8010	1000	1000
BCN20000 [14]	-	4	Nevus, Basal Cell Carcinoma Melanoma, Actinic/Seborrheic Keratosis	4800	800	800
PAD-UFES-20 [62]	-	2	Basal/Squamous Cell Carcinoma, Actinic/Seborrheic Keratosis	1602	200	200
Melanoma [36]	-	2	Benign, Malignant	8605	1000	1000
UWaterloo [45]	-	2	melanoma, not melanoma	166	20	20

Table 6: Detailed statistics of the 10 Skin Lesion datasets evaluated in this work.

626 Table 5 and 6 show the detailed statistics for all 20 datasets evaluated in this paper, where we list the  
627 number of classes with class names, the number of images for training, validation, and testing. For  
628 confounded datasets, here we explain some details about how we define the confounding factors:

- 629 • **NIH-sex** and **ISIC-sex** are built based on the patient sex from NIH-CXR [83] and ISIC.
- 630 • **NIH-age** defines young as patient’s age  $\leq 30$  and old as patient’s age  $\geq 60$ .
- 631 • **NIH-pos** refers to the patient’s position during an X-ray procedure. The standard position, Posterior  
632 Anterior (PA), involves the patient standing, while the Anterior-Posterior (AP) view is used when  
633 the patient cannot stand and must lie down.
- 634 • **CheXpert-race** selects racial subgroups (White, Black or African American) from CheXpert [35].
- 635 • **NIH-CheXpert** confounds classes by sourcing X-rays from either the NIH-CXR or CheXpert  
636 datasets. Specifically, data for one disease is obtained from one dataset, while data for a different  
637 disease is sourced from the other dataset.



Model	Pneumonia		COVID-QU		NIH-CXR		Open-i		VinDr-CXR		Average	
	ZS	LP	ZS	LP	ZS	LP	ZS	LP	ZS	LP	ZS	LP
Random	50.0	50.0	25.0	25.0	16.7	16.7	33.0	33.0	14.3	14.3	27.8	27.8
DenseNet	-	83.8	-	82.9	-	53.0	-	63.8	-	27.4	-	62.2
OpenAI-CLIP	62.5	82.4	6.7	91.0	35.0	49.6	21.6	60.3	16.0	33.1	28.4	63.3
OpenCLIP	62.5	77.4	6.3	90.0	7.5	47.9	21.6	58.7	15.4	34.9	22.7	61.8
PubMedCLIP	63.3	72.9	22.0	87.7	30.4	47.7	26.4	59.6	15.4	26.9	31.5	58.9
BioMedCLIP	74.0	85.4	11.8	90.3	31.4	58.7	56.0	67.6	22.3	36.6	39.1	67.7
PMC-CLIP	57.7	84.9	48.1	<u>94.9</u>	40.4	60.6	57.6	67.4	16.0	42.3	43.9	70.0
MedCLIP	<b>84.9</b>	<b>89.9</b>	<b>68.6</b>	87.4	25.1	64.8	<b>70.2</b>	71.9	<u>24.6</u>	40.0	<u>54.7</u>	70.8
Ours	<u>77.7</u>	88.6	<u>60.6</u>	<u>94.9</u>	<b>47.4</b>	<b>68.4</b>	<u>67.5</u>	<b>73.3</b>	<b>29.1</b>	<b>44.0</b>	<b>56.5</b>	<b>73.8</b>
– Extraction	57.2	<u>88.8</u>	46.0	<b>95.3</b>	<u>41.4</u>	<u>68.2</u>	62.9	<u>72.1</u>	21.1	<u>46.0</u>	45.7	<b>74.3</b>

Model	HAM10000		BCN20000		PAD-UFS-20		Melanoma		UWaterloo		Average	
	ZS	LP	ZS	LP	ZS	LP	ZS	LP	ZS	LP	ZS	LP
Random	14.3	14.3	25.0	25.0	50.0	50.0	50.0	50.0	50.0	50.0	37.9	37.9
DenseNet	-	79.0	-	69.6	-	69.5	-	91.9	-	45.0	-	71.0
OpenAI-CLIP	3.6	79.9	28.3	67.9	47.0	84.5	50.9	91.6	50.0	60.0	35.9	76.8
OpenCLIP	5.2	82.2	25.0	67.8	45.0	83.5	50.1	92.6	55.0	80.0	36.1	81.2
PubMedCLIP	4.8	76.3	28.9	64.4	50.5	85.5	48.8	92.2	50.0	60.0	36.6	75.7
BioMedCLIP	<u>60.4</u>	75.2	27.5	61.8	<b>61.0</b>	84.5	57.3	90.0	50.0	65.0	51.2	75.3
PMC-CLIP	25.1	82.4	24.8	67.6	55.0	86.0	66.1	92.7	55.0	55.0	45.2	76.7
MedCLIP	8.5	71.4	22.6	55.1	50.0	71.0	50.1	89.9	50.0	50.0	36.2	67.5
Ours	<b>61.5</b>	<u>82.9</u>	<b>53.0</b>	<u>71.0</u>	<u>56.5</u>	<b>86.5</b>	<b>84.0</b>	<u>93.5</u>	<b>75.0</b>	<b>80.0</b>	<b>66.0</b>	<b>82.8</b>
– Extraction	50.9	<b>83.3</b>	<u>46.5</u>	<b>72.0</b>	52.0	<b>86.5</b>	<u>80.1</u>	<b>96.0</b>	<u>70.0</u>	<u>70.0</u>	<u>59.9</u>	<u>81.6</u>

Table 7: Zero-shot (ZS) and Linear Probe (LP) results of different models on five chest X-ray and five skin lesion datasets (not confounded, random split). The best score is **bold**, and the second best is underlined. – Extraction stands for not using LLM to extract findings from clinical reports.

- **ISIC-age** thresholds young as patient’s age  $\leq 30$  and old as patient’s age  $\geq 70$ .
- **ISIC-site** focuses on lesions located either on the head or an extremity.
- **ISIC-color** organizes images based on the Fitzpatrick scale of skin tones [19]. Fitzpatrick I is classified as light skin, and III, IV, and V as dark skin, according to the annotations from [4].
- **ISIC-hospital** introduces confounds in classes by using lesion images exclusively from either the Hospital Clínic de Barcelona or the Medical University of Vienna.

## B Implementation Details

### B.1 CLIP Pretraining

We experimented with existing CLIP models in the medical domain and found their performance to be unreliable. Therefore, we decide to train our own CLIP models for X-ray and skin lesion images.

**Pretraining Dataset.** For X-rays, we utilize the MIMIC-CXR dataset [37], specifically selecting only the PA and AP X-rays, which results in 243,334 images, each accompanied by a clinical report written by doctors. For Skin Lesion images, we employ the ISIC dataset and use GPT-4V [61] to generate clinical reports for 56,590 images, examples are shown in Figure 9. We preprocess these reports by extracting medically relevant findings, each described in a short and concise term. The example below demonstrates a report alongside the findings captured by GPT-4. In total, we assemble 953K image-text pairs for X-rays and 438K for skin lesion images.

**FINAL REPORT HISTORY:** Unresponsive. Evaluate for pneumonia.  
**COMPARISON:** Chest radiographs \_\_\_\_ and \_\_\_\_\_. CT thoracic spine \_\_\_\_.  
**FINDINGS:** Portable frontal view of the chest. The lung volumes are low. No pleural effusion or pneumothorax. There is bibasilar atelectasis, left greater than right. Heart size is normal. Mediastinal and hilar structures are unremarkable. The configuration of the trachea is unchanged from prior cross-sectional imaging.  
**IMPRESSION:** Low lung volumes without an acute cardiopulmonary process.  
**FINDINGS (GPT-4):** low lung volumes, bibasilar atelectasis, left greater than right, normal heart size, trachea unchanged

**Training Details.** We utilize the training script from OpenCLIP [34] and select ViT-L/14 as the backbone. Training is performed on 4 RTX A6000 GPUs for 10 epochs with a batch size of 128 and a learning rate of  $1e^{-5}$ . We choose checkpoints based on the lowest contrastive loss on validation sets.

**CLIP Baselines.** We compare various CLIP models across unconfounded datasets for two modalities, including OpenAI-CLIP [64], OpenCLIP [34], PubMedCLIP [18], BioMedCLIP [92], PMC-CLIP<sup>1</sup> and MedCLIP [85]. We evaluate these models in both zero-shot and linear probe scenarios. In zero-shot, GPT-4 generates prompts for each class, and we use the ensemble of cosine similarities between the image and prompts as the score for each class. In linear probing, we use the CLIP models as image encoders to extract features for logistic regression. Additionally, we include DenseNet-121 [32] (fine-tuned on the pretraining datasets with cross-entropy loss) as a baseline for linear probing.

**Results.** Figure 7 shows that our CLIP models perform best in both zero-shot and linear probing scenarios for both modalities. We find that preprocessing the text data with an LLM significantly enhances zero-shot performance. Existing medical CLIP models outperform general CLIP models on X-ray datasets but not on skin lesion images, possibly because X-ray data are more prevalent and accessible in the medical domain. While our CLIP models excel with careful data curation, training converges quickly, suggesting the current contrastive objective might not fully exploit the information from the data, potentially taking shortcuts, such as comparing images from different patients instead of focusing on diseases. Future research should explore more suitable objectives and larger-scale data collections to develop more robust medical foundation models.

## B.2 Baselines

This section outlines the implementation details of all baselines compared with our knowledge bottlenecks for medical image classification. All baselines are run on a single RTX A6000 GPU.

- **ViT-L/14:** We utilize the visual encoders from the CLIP models we pretrained in Sec B.1 and add a classification head for downstream classification datasets. We unfreeze the ViT-L/14 backbone and train all parameters with a learning rate of  $1e^{-6}$  and a batch size of 64 for 20 epochs.
- **DenseNet-121:** Similarly to ViT-L/14, we add a classification head to the pretrained DenseNet and train the entire network end-to-end. For X-rays, we use the DenseNet pretrained on MIMIC-CXR by TorchXRyVision [13]. For skin lesion images, we pre-train the DenseNet from scratch on ISIC using a cross-entropy loss. When fine-tuned for downstream classification datasets, we train the DenseNet with a learning rate of  $1e^{-5}$ , a batch size of 64, and also for 20 epochs.
- **Linear Probe:** We employ visual encoders (ViT-L/14) from pretrained CLIP models to extract features for images in downstream classification datasets. We train a linear layer to map these features into labels for 200 epochs with a learning rate of  $1e^{-3}$  and a batch size of 64.
- **LSL [56]:** We fine-tune the pretrained CLIP with contrastive loss on annotated concept data (PubMed bottleneck), using the same data as for concept grounding functions (4.3). Training instances are triplets  $(I, c, y)$ , where  $I$  is the image,  $c$  is a textual concept, and  $y \in \{0, 1\}$  is a binary label indicating whether the image contains this concept. Given the visual encoder  $\mathcal{V}$  and textual encoder  $\mathcal{T}$  of the CLIP, the cosine similarity between an image and a concept is  $s(I, c) = \cos(\mathcal{V}(I), \mathcal{T}(c))$ . The contrastive loss function is defined as  $\mathcal{L}_{\text{contrast}} = y \cdot \max(0, m - s(I, c)) + (1 - y) \cdot s(I, c)$ , where  $m = 0.6$  is the margin. We fine-tune the CLIP with concept annotations for 20 epochs with a learning rate of  $1e^{-6}$  and a batch size of 64. After obtaining the fine-tuned CLIP, we extract features and train a linear probe in the same manner as the linear probe baseline.
- **PCBM-h [91] and LaBo [90]:** We use their codebases to implement these baselines. The concept alignment in both models is achieved using CLIP to compute the dot product between image and concept features. PCBM-h uses the same bottleneck as KnoBo, which is generated from PubMed. For LaBo, we employ GPT-4 to generate candidate concepts for submodular selection.

## B.3 KnoBo Details

This section provides additional details about the implementation of KnoBo.

**Medical Corpus.** We utilize a comprehensive medical corpus for retrieval-augmented generation, detailed as follows: (1) PubMed (5.5M docs, 156.9M snippets); (2) StatPearls (9.3K docs, 301.2K

<sup>1</sup>[https://huggingface.co/ryanyip7777/pmc\\_vit\\_l\\_14](https://huggingface.co/ryanyip7777/pmc_vit_l_14)

You are an experienced radiologist [dermatologist]. You are summarizing knowledge about '**QUERY**' from chest X-rays [skin lesion images]. Here are the documents retrieved from the corpus:

#### RETRIEVED\_DOCUMENTS

I want you to filter and summarize the information in these documents and generate knowledge in the form of \*binary questions\*, e.g., "Is there lung opacity?" ["Is the lesion asymmetric?"].

Please follow instructions below strictly:

1. Those knowledge will be used to guide the diagnosis on chest X-rays [skin lesion images], so they must be \*visually identifiable\* from chest X-ray [skin lesion images] only.
2. The binary questions should be concise and not too specific which can be reused for different cases.
3. The binary questions must not contain the class(disease) name, e.g., you \*must not\* generate "Is there cardiomegaly?" ["Is the lesion malignant?"] as the knowledge for "Cardiomegaly" ["Malignant Lesion"].
4. If there is not much information in the some documents, you can ignore those documents. If none of the documents contain useful information, you can skip this task by typing 'skip'.
5. Answer with the following format: question | document ID | reference sentence, e.g., Is there lung opacity? | 1234 | lung opacity is a common finding for ... [Is the lesion asymmetric? | 1234 | asymmetric lesion is a common finding for ...]

Please answer without additional information and do not add numbers or bullet points in the answer.

Figure 5: Prompt template for retrieval-augmented concept bottleneck generation. The text in the square brackets is words that need to be changed when using this prompt for skin lesion images.

LLM	Chest X-ray Datasets						Skin Lesion Datasets					
	ID	OOD	$\Delta \downarrow$	Avg	Unconfound	Overall	ID	OOD	$\Delta \downarrow$	Avg	Unconfound	Overall
Flan-T5	89.7	<b>58.8</b>	<b>30.9</b>	<b>74.3</b>	<b>73.1</b>	<b>73.7</b>	<b>86.0</b>	70.5	14.1	78.3	78.1	78.2
GPT-4	<b>89.9</b>	56.8	33.1	73.3	72.9	73.1	<b>86.0</b>	<b>71.6</b>	<b>14.4</b>	<b>78.8</b>	<b>78.5</b>	<b>78.6</b>

Table 8: Comparison of using different LLM annotating concepts on clinical reports.

snippets); (3) Textbooks (18 docs, 125.8K snippets); (4) Wikipedia (6.5M docs, 29.9M snippets). The StatPearls, Textbooks, and Wikipedia sources are obtained from MEDRAG [88]. Unlike the abstract-only approach of PubMed in MEDRAG, we utilize full articles from PubMed, including all paragraphs. We employ the retrieval codebase of MEDRAG and select BM25 as the ranking function.

**Retrieval-augmented Concept Bottleneck Generation.** Figure 5 illustrates the prompt template we use to generate concepts from documents. We retrieve the top 10 documents for each query as context for the large language model (GPT-4) to generate concepts. After generating concepts, we validate each concept based on three criteria before inclusion in the bottleneck: (1) the concept must be distinct from existing concepts; (2) it must be visually identifiable from the image; and (3) there must be sufficient positive and negative instances in the pretraining corpus to support training its grounding function. A concept is added to the bottleneck only if it meets all three criteria, as judged by another language model (GPT-4). We initially target 200 concepts per bottleneck but ultimately select the top 150 with the highest grounding accuracy for inclusion. This selection is due to some concepts lacking sufficient reports to effectively train their grounding functions, making 150 the minimum size for all the bottlenecks we construct. Table 12 shows examples of generated concepts.

**Concept Grounding.** We use a language model to annotate 2,000 clinical reports for each concept from the pretraining corpus. To efficiently label reports and achieve a balance of positive and negative examples, we retrieve the top 1,000 reports showing high textual similarity (measured by Sentence Transformer [65]) to the concept as its potential positive examples and randomly sample another 1,000 for potential negatives. We use Flan-T5-XXL [10] as the underlying large language model. Specifically, the annotation task is treated as a next token prediction, similar to the approach proposed by McInerney et al. [54], where we compare the probabilities of the next token being Yes or No to determine if the report contains the concept. Figure 8 shows no big difference in final classification performance when using Flan-T5 versus GPT-4 for annotating concepts on reports.

## C Additional Analysis

This section presents additional analysis and ablation studies on our method.

### C.1 Details about Deep Image Priors

We provide further details about the deep image prior experiments in Sec 3.

Feature	Natural Image Datasets					
	CIFAR-10	STL-10	ImageNet-10	Food-101	Flower-102	Average
Random	10.0	10.0	10.0	1.0	1.0	6.4
Pixel Value	21.2	24.7	22.4	3.0	8.5	16.0
ConvNext-L*	25.6	29.1	32.6	3.7	11.3	20.5
ViT-L/14*	<b>33.3</b>	<b>40.6</b>	<b>47.2</b>	<b>8.9</b>	<b>23.6</b>	<b>30.7</b>

Feature	X-ray Datasets					
	Pneumonia	COVID-QU	NIH-CXR	Open-i	VinDr-CXR	Average
Random	50.0	25.0	16.7	33.0	14.3	27.8
Pixel Value	<b>77.6</b>	66.9	<b>43.1</b>	<b>58.3</b>	<b>20.0</b>	<b>53.2</b>
ConvNext-L*	62.5	59.2	38.9	57.5	<b>20.0</b>	47.6
ViT-L/14*	67.6	<b>68.0</b>	40.4	57.2	<b>20.0</b>	50.6

Feature	Skin Lesion Datasets					
	HAM10000	BCN20000	PAD-UFS-20	Melanoma	UWaterloo	Average
Random	14.3	25.0	50.0	50.0	50.0	37.9
Pixel Value	65.9	39.4	<b>58.0</b>	74.5	<b>70.0</b>	<b>61.6</b>
ConvNext-L*	66.9	37.1	53.5	68.3	50.0	55.8
ViT-L/14*	<b>67.3</b>	<b>45.9</b>	54.0	<b>84.8</b>	50.0	61.5

Table 9: Linear Probe results of different features on five natural image datasets, five X-ray datasets, and five skin lesion datasets. \* denotes the network is randomly initialized without any training.

**Datasets.** We evaluate the deep image prior on three categories of images. The X-ray and skin lesion images are the same as those described in the unconfounded datasets section (Sec A). For natural images, we select five datasets: (1) CIFAR-10 [43], (2) STL-10 [11], (3) ImageNet-10 [70]<sup>2</sup>, (4) Food-101 [7], and (5) Flower-102 [59].

**Setup.** We employ the vision backbones ViT-L/14 [17] and ConvNext-L [51], both implemented by OpenCLIP [34], and initialize them using Kaiming initialization [28] following PyTorch’s default settings<sup>3</sup>. Both backbones extract feature vectors of size 768. For the pixel value baseline, we convert the image to grayscale, resize it to  $28 \times 28$ , and then flatten it into a vector of 784 dimensions. We use the first 768 values of this pixel vector to match the size of the deep features. All features are passed through a linear layer to predict the labels with a learning rate of  $1e^{-3}$ , a batch size of 64 for 200 epochs. Additionally, we include a random baseline for comparison.

**Results.** Table 9 displays the full results of all methods across the three image categories. ViT-L/14 excels on natural datasets with significant gains over pixel baselines. ConvNext-L performs worse than ViT-L/14 but is still notably more effective than pixel-based methods. For X-ray images, the pixel baseline clearly surpasses the two networks on almost all datasets, indicating that deep models lack priors or even have harmful priors for X-ray imaging. For skin lesion images, which are closer to natural images, the pixel value baseline performs comparably to ViT-L/14 and better than ConvNext-L. Overall, the results suggest that deep networks lack sufficient priors for medical domains, potentially affecting their generalizability.

## C.2 Full Results on Unconfounded Datasets

Table 10 shows the comprehensive results of all baselines across the 10 unconfounded medical datasets. KnoBo performs competitively in the X-ray category, securing top-1 positions for two datasets and achieving an average ranking of third among all methods. For skin lesion datasets, KnoBo’s performance is limited by the smaller scale and lower quality of the pretraining corpus, which is annotated by GPT-4V rather than by human experts. This affects the effectiveness of the grounding functions for lesion concepts. With access to larger-scale and higher-quality pretraining data, KnoBo could potentially close the performance gap with black-box baselines.

<sup>2</sup>We use the 10 classes selected by Imagenette: <https://github.com/fastai/imagenette>.

<sup>3</sup><https://pytorch.org/docs/stable/nn.init.html>

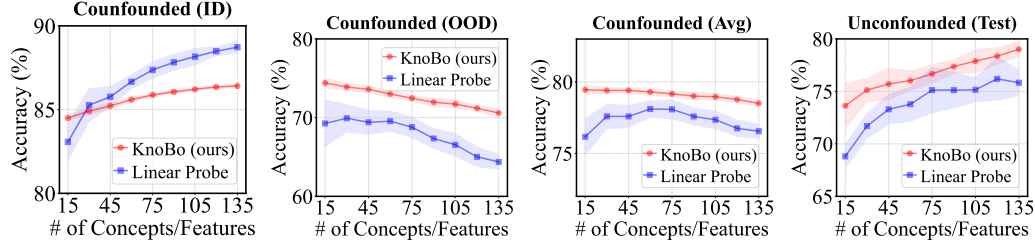


Figure 6: Ablation of **bottleneck** sizes on Skin Lesion datasets. The x-axis is the number of randomly selected concepts (KnoBo) or visual features (Linear Probe). We report the ID, OOD, and domain-average performance on confounded datasets and test the accuracy of the unconfounded datasets.

Method	Chest X-ray Standard Datasets					
	Pneumonia	COVID-QU	NIH-CXR	Open-i	VinDr-CXR	Average
ViT-L/14	84.6	<b>96.5</b>	66.0	67.0	37.1	70.2
DenseNet	85.1	92.4	56.9	63.5	32.0	66.0
Linear Probe	88.6	94.9	68.4	73.3	44.0	73.8
LSL	87.0	86.9	58.4	64.8	37.7	67.0
PCBM-h	87.7	94.9	<b>68.6</b>	73.2	<b>49.1</b>	<b>74.7</b>
LaBo	88.3	91.8	66.8	68.9	44.6	72.1
KnoBo (ours)	<b>90.1</b>	88.0	66.5	<b>73.5</b>	47.4	73.1

Method	Skin Lesion Standard Datasets					
	HAM10000	BCN20000	PAD-UFS-20	Melanoma	UWaterloo	Average
ViT-L/14	<b>87.1</b>	<b>76.6</b>	<b>88.5</b>	<b>94.1</b>	75.0	<b>84.3</b>
DenseNet	79.0	69.6	69.5	91.9	45.0	71.0
Linear Probe	82.9	71.0	86.5	93.5	<b>80.0</b>	82.8
LSL	81.5	67.5	84.5	92.5	60.0	77.2
PCBM-h	82.9	70.9	86.0	93.6	75.0	81.7
LaBo	80.6	68.5	82.5	93.6	75.0	80.0
KnoBo (ours)	78.2	65.6	80.0	91.5	75.0	78.1

Table 10: Test accuracy on 10 **unconfounded** datasets of two modalities.

### C.3 Ablate Bottleneck Size for Skin Lesion

Figure 6 compares the performance of KnoBo and a Linear Probe across different feature sizes on skin lesion datasets. Mirroring the trends observed in X-rays shown in Figure 4, our interpretable bottleneck representations consistently outperform black-box visual features.

### C.4 Human Evaluation on Bottlenecks

Two medical students evaluated the quality of bottlenecks using two metrics: (1) **Relevance** measures the concept’s relevance to diagnosing diseases on a scale from 1 (not at all relevant) to 4 (mostly relevant), and (2) **Groundability** assesses the verifiability of the concept from the image on a scale from 1 to 4. We evaluated 30 randomly sampled concepts from each bottleneck. Table 11 presents these metrics for bottlenecks constructed from five different knowledge sources. While all bottlenecks show good relevance, groundability scores are lower, reflecting the challenge of deriving visual concepts from text-only data.

Table 11: Relevance and Groundability of concepts in bottlenecks generated from different resources, as evaluated by student doctors.

Knowledge Source	Relevance		Groundability	
	X-ray	Skin	X-ray	Skin
PROMPT	3.83	3.93	3.03	3.00
TEXTBOOKS	3.70	3.80	2.90	3.27
WIKIPEDIA	3.80	3.67	2.83	3.33
STATPEARLS	3.87	3.80	2.70	2.97
PUBMED	3.70	3.83	2.77	3.20







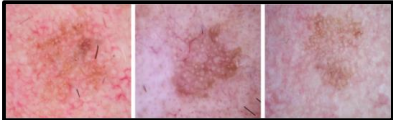
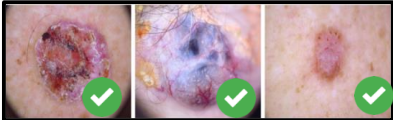
Query		CLIP	Ours (w/ concept grounding)
<i>Are lung fields clear on both sides?</i>	Top-3		
<i>Is there a visible enlargement of the heart?</i>	Top-3		
<i>Does the lesion have a regularly shaped border?</i>	Top-3		
<i>Does the lesion show dry scaly areas?</i>	Top-3		

Figure 7: Compare CLIP and our concept grounding function in retrieving images based on a text query. Images marked with green checkmarks are correct retrievals as assessed by medical students.



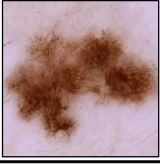
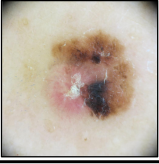
NIH-CXR	<b>Edema</b>	<b>Top-3 Concepts</b>
		<ul style="list-style-type: none"> <li>Are abnormalities observed in the subpleural region?</li> <li>Are there new alveolar or interstitial infiltrates?</li> <li>Are any areas of hazy opacity present?</li> </ul>
VinDr-CXR	<b>Cardiomegaly</b>	<b>Top-3 Concepts</b>
		<ul style="list-style-type: none"> <li>Is there an enlarged cardiac silhouette?</li> <li>Can increased cardiothoracic ratios be identified?</li> <li>Does the radiograph show any large transverse dimension of the heart?</li> </ul>
Melanocytic Nev	<b>Melanocytic Nev</b>	<b>Top-3 Concepts</b>
		<ul style="list-style-type: none"> <li>Does the lesion appear as an elevated nodule?</li> <li>Does the lesion have an asymmetric disposition?</li> <li>Can brownish-black verrucose plaques be seen on the body?</li> </ul>
BCN2000	<b>Melanoma</b>	<b>Top-3 Concepts</b>
		<ul style="list-style-type: none"> <li>Does the lesion present as a flat pigmented area?</li> <li>Does the lesion adhere to the ABCD dermoscopy rule?</li> <li>Does the lesion show central ulceration-crust?</li> </ul>

Figure 8: Top-3 concepts for a class ranked by their weights in the linear layer of KnoBo.

## D Qualitative Examples

Figure 7 compares the CLIP dot product and our concept grounding functions for retrieving images based on text queries. Our method demonstrates superior recall of correct examples compared to CLIP alignments. Figure 8 showcases the top concepts selected based on the linear weights learned by KnoBo, which are most correlated with the corresponding disease class. These examples highlight that the top concepts utilized by KnoBo are essential features doctors use for diagnosing targeted diseases. Table 12 displays examples of concepts generated by our retrieval-augmented approach. Each concept can be traced back to its source document to verify its accuracy. Figure 9 presents examples of GPT-4V-annotated clinical reports for skin lesion images. Notably, the second example demonstrates GPT-4V’s capability to assess lesion size using the scale provided in the image.

Bottleneck	Concept	Query	Reference Document
X-ray (PubMed)	Is there lung collapse?	Atelectasis	Atelectasis and pneumonia were diagnosed on radiological and clinical criteria. <b>Atelectasis was diagnosed when a finding of lung collapse was made on chest X-ray</b> , chest CT and/or lung ultrasound. [Source]
X-ray (StatPearls)	Is there a widened mediastinum on chest X-ray?	Aortic Enlargement	On chest x-ray (CXR), <b>findings that may indicate aortic pathology include a widened mediastinum</b> , loss of the aortic knob contour, inferiorly displaced left bronchus, and left pleural effusion. [Source]
Skin (Textbook)	Does the lesion have a waxy appearance?	Seborrheic Keratosis	Lesions have no malignant potential but may be a cosmetic problem. <b>Present as exophytic, waxy brown papules and plaques with prominent follicle openings</b> . [In the book: First Aid Step-2]
Skin (Wikipedia)	Are there small blood vessels running over the skin lesion?	Basal Cell Carcinoma	BCC, also known as basal-cell cancer, is the most common type of skin cancer. It often appears as a painless raised area of skin, <b>which may be shiny with small blood vessels running over it</b> . [Source]

Table 12: We show concepts from various bottlenecks by image modality (corpus), with the queries for retrieval and the corresponding reference documents to generate the concept. Every concept is attributable, allowing medical professionals to verify its origin in the supporting documentation.


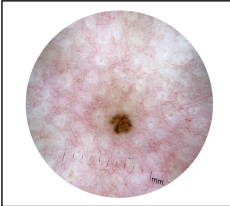
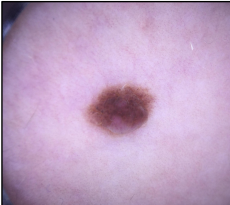
	<p>Location: Lower extremity</p> <p>Lesion Description: Macroscopic Characteristics: The lesion presents as a solitary macule with a relatively homogeneous area centrally and a slightly <b>irregular periphery</b>.</p> <p>Color: <b>Tan to light brown</b> background with <b>several shades of light to dark brown pigmentation centrally</b>.</p> <p>Networks: A faint reticular pattern is seen in portions of the lesion, with the network <b>fading towards the edges</b>.</p> <p>Structures and Patterns: Focal areas exhibit a more globular pattern, while the majority of the lesion lacks specific structural components.</p> <p>Symmetry: The lesion exhibits <b>asymmetry</b> in both color and structure.</p> <p>Borders: <b>Borders are ill-defined</b>, with the pigment diffusing into the surrounding skin.</p>
	<p>The lesion presents as a well-circumscribed, ovoid macule measuring <b>approximately 2.7mm</b> in its largest diameter, located on the posterior torso. Dermoscopically, it is characterized by a homogenous pattern with a <b>central brown pigmentation</b> that shows a subtle variegation in color intensity, ranging from light to darker brown. The peripheral area of the lesion <b>transitions to a lighter, more tan hue</b>, with discrete fading into the surrounding normal skin without evidence of a sharp border.</p> <p>Vascular structures are not prominent within the lesion itself; however, the background skin exhibits a reticular pattern of <b>superficial blood vessels</b> which is consistent with the anatomical site and possibly the patient's age. There is no evidence of atypical pigment networks, blue-whitish veils, regression structures, or other sinister features typically associated with malignancy.</p>
	<p>General Appearance: The lesion appears as a <b>well-defined, round to oval</b> macule with a notable central darker area and a lighter peripheral zone. It measures approximately 1 cm in diameter.</p> <p>Color: The lesion exhibits a heterogeneous mix of <b>dark brown and tan shades</b>. The <b>central area is densely pigmented</b>, surrounded by a less intensely colored periphery.</p> <p>Texture: The surface texture cannot be precisely determined from the image alone, but there appears to be no significant elevation or depression compared to the surrounding skin.</p> <p>Distribution and Symmetry: The lesion is solitary with a <b>symmetrical appearance</b>.</p> <p>Additional Observations: No visible scales, ulcers, or signs of bleeding are present. Hair follicles can be observed within and around the lesion, suggesting it is not disrupting normal skin structures significantly.</p>

Figure 9: Examples of clinical reports on skin lesion images generated by GPT-4V [61].

## NeurIPS Paper Checklist

### 1. Claims

Question: Do the main claims made in the abstract and introduction accurately reflect the paper's contributions and scope?

Answer: [Yes]

Justification: The main claims are limited to our specific experiments and focus on the behavior of our models.

Guidelines:

- The answer NA means that the abstract and introduction do not include the claims made in the paper.
- The abstract and/or introduction should clearly state the claims made, including the contributions made in the paper and important assumptions and limitations. A No or NA answer to this question will not be perceived well by the reviewers.
- The claims made should match theoretical and experimental results, and reflect how much the results can be expected to generalize to other settings.
- It is fine to include aspirational goals as motivation as long as it is clear that these goals are not attained by the paper.

### 2. Limitations

Question: Does the paper discuss the limitations of the work performed by the authors?

Answer: [Yes]

Justification: Limitations are discussed in the corresponding section.

Guidelines:

- The answer NA means that the paper has no limitation while the answer No means that the paper has limitations, but those are not discussed in the paper.
- The authors are encouraged to create a separate "Limitations" section in their paper.
- The paper should point out any strong assumptions and how robust the results are to violations of these assumptions (e.g., independence assumptions, noiseless settings, model well-specification, asymptotic approximations only holding locally). The authors should reflect on how these assumptions might be violated in practice and what the implications would be.
- The authors should reflect on the scope of the claims made, e.g., if the approach was only tested on a few datasets or with a few runs. In general, empirical results often depend on implicit assumptions, which should be articulated.
- The authors should reflect on the factors that influence the performance of the approach. For example, a facial recognition algorithm may perform poorly when image resolution is low or images are taken in low lighting. Or a speech-to-text system might not be used reliably to provide closed captions for online lectures because it fails to handle technical jargon.
- The authors should discuss the computational efficiency of the proposed algorithms and how they scale with dataset size.
- If applicable, the authors should discuss possible limitations of their approach to address problems of privacy and fairness.
- While the authors might fear that complete honesty about limitations might be used by reviewers as grounds for rejection, a worse outcome might be that reviewers discover limitations that aren't acknowledged in the paper. The authors should use their best judgment and recognize that individual actions in favor of transparency play an important role in developing norms that preserve the integrity of the community. Reviewers will be specifically instructed to not penalize honesty concerning limitations.

### 3. Theory Assumptions and Proofs

Question: For each theoretical result, does the paper provide the full set of assumptions and a complete (and correct) proof?

Answer: [NA]



Justification: The paper contains no theoretical results or proofs.

Guidelines:

- The answer NA means that the paper does not include theoretical results.
- All the theorems, formulas, and proofs in the paper should be numbered and cross-referenced.
- All assumptions should be clearly stated or referenced in the statement of any theorems.
- The proofs can either appear in the main paper or the supplemental material, but if they appear in the supplemental material, the authors are encouraged to provide a short proof sketch to provide intuition.
- Inversely, any informal proof provided in the core of the paper should be complemented by formal proofs provided in appendix or supplemental material.
- Theorems and Lemmas that the proof relies upon should be properly referenced.

#### 4. Experimental Result Reproducibility

Question: Does the paper fully disclose all the information needed to reproduce the main experimental results of the paper to the extent that it affects the main claims and/or conclusions of the paper (regardless of whether the code and data are provided or not)?

Answer: [Yes]

Justification: Major details are supplied in the main body, while more minor ones are in the appendix.

Guidelines:

- The answer NA means that the paper does not include experiments.
- If the paper includes experiments, a No answer to this question will not be perceived well by the reviewers: Making the paper reproducible is important, regardless of whether the code and data are provided or not.
- If the contribution is a dataset and/or model, the authors should describe the steps taken to make their results reproducible or verifiable.
- Depending on the contribution, reproducibility can be accomplished in various ways. For example, if the contribution is a novel architecture, describing the architecture fully might suffice, or if the contribution is a specific model and empirical evaluation, it may be necessary to either make it possible for others to replicate the model with the same dataset, or provide access to the model. In general, releasing code and data is often one good way to accomplish this, but reproducibility can also be provided via detailed instructions for how to replicate the results, access to a hosted model (e.g., in the case of a large language model), releasing of a model checkpoint, or other means that are appropriate to the research performed.
- While NeurIPS does not require releasing code, the conference does require all submissions to provide some reasonable avenue for reproducibility, which may depend on the nature of the contribution. For example
  - (a) If the contribution is primarily a new algorithm, the paper should make it clear how to reproduce that algorithm.
  - (b) If the contribution is primarily a new model architecture, the paper should describe the architecture clearly and fully.
  - (c) If the contribution is a new model (e.g., a large language model), then there should either be a way to access this model for reproducing the results or a way to reproduce the model (e.g., with an open-source dataset or instructions for how to construct the dataset).
  - (d) We recognize that reproducibility may be tricky in some cases, in which case authors are welcome to describe the particular way they provide for reproducibility. In the case of closed-source models, it may be that access to the model is limited in some way (e.g., to registered users), but it should be possible for other researchers to have some path to reproducing or verifying the results.

#### 5. Open access to data and code

Question: Does the paper provide open access to the data and code, with sufficient instructions to faithfully reproduce the main experimental results, as described in supplemental material?

Answer: [Yes]

Justification: The code is provided in the submission as a zip file, and we will release the code and data on Git Hub after review.

Guidelines:

- The answer NA means that paper does not include experiments requiring code.
- Please see the NeurIPS code and data submission guidelines (<https://nips.cc/public/guides/CodeSubmissionPolicy>) for more details.
- While we encourage the release of code and data, we understand that this might not be possible, so “No” is an acceptable answer. Papers cannot be rejected simply for not including code, unless this is central to the contribution (e.g., for a new open-source benchmark).
- The instructions should contain the exact command and environment needed to run to reproduce the results. See the NeurIPS code and data submission guidelines (<https://nips.cc/public/guides/CodeSubmissionPolicy>) for more details.
- The authors should provide instructions on data access and preparation, including how to access the raw data, preprocessed data, intermediate data, and generated data, etc.
- The authors should provide scripts to reproduce all experimental results for the new proposed method and baselines. If only a subset of experiments are reproducible, they should state which ones are omitted from the script and why.
- At submission time, to preserve anonymity, the authors should release anonymized versions (if applicable).
- Providing as much information as possible in supplemental material (appended to the paper) is recommended, but including URLs to data and code is permitted.

## 6. Experimental Setting/Details

Question: Does the paper specify all the training and test details (e.g., data splits, hyper-parameters, how they were chosen, type of optimizer, etc.) necessary to understand the results?

Answer: [Yes]

Justification: All details for experiments are supplied in the main body and appendix.

Guidelines:

- The answer NA means that the paper does not include experiments.
- The experimental setting should be presented in the core of the paper to a level of detail that is necessary to appreciate the results and make sense of them.
- The full details can be provided either with the code, in appendix, or as supplemental material.

## 7. Experiment Statistical Significance

Question: Does the paper report error bars suitably and correctly defined or other appropriate information about the statistical significance of the experiments?

Answer: [Yes]

Justification: Figure 4 and 6 have error bars. Broadly, the paper covers many datasets and reports each individually. This provides enough information about the variance of the approach. We do not rerun methods on each dataset as this would be computationally wasteful.

Guidelines:

- The answer NA means that the paper does not include experiments.
- The authors should answer "Yes" if the results are accompanied by error bars, confidence intervals, or statistical significance tests, at least for the experiments that support the main claims of the paper.
- The factors of variability that the error bars are capturing should be clearly stated (for example, train/test split, initialization, random drawing of some parameter, or overall run with given experimental conditions).

- The method for calculating the error bars should be explained (closed form formula, call to a library function, bootstrap, etc.)
- The assumptions made should be given (e.g., Normally distributed errors).
- It should be clear whether the error bar is the standard deviation or the standard error of the mean.
- It is OK to report 1-sigma error bars, but one should state it. The authors should preferably report a 2-sigma error bar than state that they have a 96% CI, if the hypothesis of Normality of errors is not verified.
- For asymmetric distributions, the authors should be careful not to show in tables or figures symmetric error bars that would yield results that are out of range (e.g. negative error rates).
- If error bars are reported in tables or plots, The authors should explain in the text how they were calculated and reference the corresponding figures or tables in the text.

## 8. Experiments Compute Resources

Question: For each experiment, does the paper provide sufficient information on the computer resources (type of compute workers, memory, time of execution) needed to reproduce the experiments?

Answer: [Yes]

Justification: This information is provided in the appendix B.

Guidelines:

- The answer NA means that the paper does not include experiments.
- The paper should indicate the type of compute workers CPU or GPU, internal cluster, or cloud provider, including relevant memory and storage.
- The paper should provide the amount of compute required for each of the individual experimental runs as well as estimate the total compute.
- The paper should disclose whether the full research project required more compute than the experiments reported in the paper (e.g., preliminary or failed experiments that didn't make it into the paper).

## 9. Code Of Ethics

Question: Does the research conducted in the paper conform, in every respect, with the NeurIPS Code of Ethics <https://neurips.cc/public/EthicsGuidelines>?

Answer: [Yes]

Justification: Having reviewed the policy, we follow all bullets across the three areas.

Guidelines:

- The answer NA means that the authors have not reviewed the NeurIPS Code of Ethics.
- If the authors answer No, they should explain the special circumstances that require a deviation from the Code of Ethics.
- The authors should make sure to preserve anonymity (e.g., if there is a special consideration due to laws or regulations in their jurisdiction).

## 10. Broader Impacts

Question: Does the paper discuss both potential positive societal impacts and negative societal impacts of the work performed?

Answer: [Yes]

Justification: This information is provided in the last section of the paper in the main body.

Guidelines:

- The answer NA means that there is no societal impact of the work performed.
- If the authors answer NA or No, they should explain why their work has no societal impact or why the paper does not address societal impact.
- Examples of negative societal impacts include potential malicious or unintended uses (e.g., disinformation, generating fake profiles, surveillance), fairness considerations (e.g., deployment of technologies that could make decisions that unfairly impact specific groups), privacy considerations, and security considerations.

- The conference expects that many papers will be foundational research and not tied to particular applications, let alone deployments. However, if there is a direct path to any negative applications, the authors should point it out. For example, it is legitimate to point out that an improvement in the quality of generative models could be used to generate deepfakes for disinformation. On the other hand, it is not needed to point out that a generic algorithm for optimizing neural networks could enable people to train models that generate Deepfakes faster.
- The authors should consider possible harms that could arise when the technology is being used as intended and functioning correctly, harms that could arise when the technology is being used as intended but gives incorrect results, and harms following from (intentional or unintentional) misuse of the technology.
- If there are negative societal impacts, the authors could also discuss possible mitigation strategies (e.g., gated release of models, providing defenses in addition to attacks, mechanisms for monitoring misuse, mechanisms to monitor how a system learns from feedback over time, improving the efficiency and accessibility of ML).

## 11. Safeguards

Question: Does the paper describe safeguards that have been put in place for responsible release of data or models that have a high risk for misuse (e.g., pretrained language models, image generators, or scraped datasets)?

Answer: [\[Yes\]](#)

Justification: We will release the data and models with an appropriate warning that these systems should not be used for any direct diagnosis without randomized trials supporting their efficacy.

Guidelines:

- The answer NA means that the paper poses no such risks.
- Released models that have a high risk for misuse or dual-use should be released with necessary safeguards to allow for controlled use of the model, for example by requiring that users adhere to usage guidelines or restrictions to access the model or implementing safety filters.
- Datasets that have been scraped from the Internet could pose safety risks. The authors should describe how they avoided releasing unsafe images.
- We recognize that providing effective safeguards is challenging, and many papers do not require this, but we encourage authors to take this into account and make a best faith effort.

## 12. Licenses for existing assets

Question: Are the creators or original owners of assets (e.g., code, data, models), used in the paper, properly credited and are the license and terms of use explicitly mentioned and properly respected?

Answer: [\[Yes\]](#)

Justification: We cite all dependencies of our work and verify that we are using their data, models, and methods in a way consistent with their terms.

Guidelines:

- The answer NA means that the paper does not use existing assets.
- The authors should cite the original paper that produced the code package or dataset.
- The authors should state which version of the asset is used and, if possible, include a URL.
- The name of the license (e.g., CC-BY 4.0) should be included for each asset.
- For scraped data from a particular source (e.g., website), the copyright and terms of service of that source should be provided.
- If assets are released, the license, copyright information, and terms of use in the package should be provided. For popular datasets, [paperswithcode.com/datasets](https://paperswithcode.com/datasets) has curated licenses for some datasets. Their licensing guide can help determine the license of a dataset.

- For existing datasets that are re-packaged, both the original license and the license of the derived asset (if it has changed) should be provided.
- If this information is not available online, the authors are encouraged to reach out to the asset’s creators.

### 13. New Assets

Question: Are new assets introduced in the paper well documented and is the documentation provided alongside the assets?

Answer: [Yes]

Justification: The paper documents our models, and our GitHub release will contain usage instructions. Novel dataset components will be released that are consistent with license instructions from base datasets.

Guidelines:

- The answer NA means that the paper does not release new assets.
- Researchers should communicate the details of the dataset/code/model as part of their submissions via structured templates. This includes details about training, license, limitations, etc.
- The paper should discuss whether and how consent was obtained from people whose asset is used.
- At submission time, remember to anonymize your assets (if applicable). You can either create an anonymized URL or include an anonymized zip file.

### 14. Crowdsourcing and Research with Human Subjects

Question: For crowdsourcing experiments and research with human subjects, does the paper include the full text of instructions given to participants and screenshots, if applicable, as well as details about compensation (if any)?

Answer: [NA]

Justification: There is no crowdsourcing or human subject research in this work.

Guidelines:

- The answer NA means that the paper does not involve crowdsourcing nor research with human subjects.
- Including this information in the supplemental material is fine, but if the main contribution of the paper involves human subjects, then as much detail as possible should be included in the main paper.
- According to the NeurIPS Code of Ethics, workers involved in data collection, curation, or other labor should be paid at least the minimum wage in the country of the data collector.

### 15. Institutional Review Board (IRB) Approvals or Equivalent for Research with Human Subjects

Question: Does the paper describe potential risks incurred by study participants, whether such risks were disclosed to the subjects, and whether Institutional Review Board (IRB) approvals (or an equivalent approval/review based on the requirements of your country or institution) were obtained?

Answer: [NA]

Justification: There is no crowdsourcing or human subject research in this work.

Guidelines:

- The answer NA means that the paper does not involve crowdsourcing nor research with human subjects.
- Depending on the country in which research is conducted, IRB approval (or equivalent) may be required for any human subjects research. If you obtained IRB approval, you should clearly state this in the paper.
- We recognize that the procedures for this may vary significantly between institutions and locations, and we expect authors to adhere to the NeurIPS Code of Ethics and the guidelines for their institution.

1104  
1105

- For initial submissions, do not include any information that would break anonymity (if applicable), such as the institution conducting the review.